JGR Atmospheres

RESEARCH ARTICLE
10.1029/2024JD041414

Response and Feedback of Mesoscale Eddies to Tropical Cyclones Over the South China Sea

Ping Liu[1], Shoude Guan[1,2,3], I.-I. Lin[4], Mengya Huang[1], Fei-Fei Jin[5], Qian Wang[6], Zhumin Lu[7], Wei Zhao[1,2,3], and Jiwei Tian[1,2,3]

[1]Frontier Science Center for Deep Ocean Multispheres and Earth System (FDOMES) and Physical Oceanography Laboratory/Key Laboratory of Ocean Observation and Information of Hainan Province, Sanya Oceanographic Institution/Academy of the Future Ocean, Ocean University of China, Qingdao/Sanya, China, [2]SANYA Oceanographic Laboratory, Sanya, China, [3]Laboratory for Ocean Dynamics and Climate, Qingdao Marine Science and Technology Center, Qingdao, China, [4]Department of Atmospheric Sciences, National Taiwan University, Taipei, Taiwan, [5]Department of Atmospheric Sciences, SOEST, University of Hawaii at Manoa, Honolulu, HI, USA, [6]National Meteorological Centre, Beijing, China, [7]State Key Laboratory of Tropical Oceanography, South China Sea Institute of Oceanology, Chinese Academy of Sciences, Guangzhou, China

Key Points:

- Tropical cyclone (TC), frequently occurring in the South China Sea, interacts with at least one mesoscale eddy during its lifespan
- TCs enhance (weaken) pre-TC cyclonic (anticyclonic) eddies by a 24% increase (17% decrease) in amplitude
- Pre-existing cyclonic (anticyclonic) eddies enhance (suppress) TC-induced cooling and suppress (fuel) TC intensification

Supporting Information:

Supporting Information may be found in the online version of this article.

Correspondence to:

S. Guan,
guanshoude@ouc.edu.cn

Citation:

Liu, P., Guan, S., Lin, I.-I., Huang, M., Jin, F.-F., Wang, Q., et al. (2025). Response and feedback of mesoscale eddies to tropical cyclones over the South China Sea. *Journal of Geophysical Research: Atmospheres*, *130*, e2024JD041414. https://doi.org/10.1029/2024JD041414

Received 19 APR 2024
Accepted 20 DEC 2024

Abstract Tropical cyclones (TCs) frequently encounter and interact with mesoscale eddies when moving over the ocean, affecting both of their subsequent evolutions. The South China Sea (SCS) suffers the most frequent TCs among global oceans and contains active eddies. On average, one TC encounters and interacts with at least one eddy during its lifespan in the SCS. Using 27-year satellite data and numerical simulations, we examined the response and feedback of mesoscale eddies to TCs over the SCS, based on TCs' interaction with 183 cyclonic ocean eddies (COEs) and 152 anticyclonic ocean eddies (AOEs). TCs induce a symmetric sea surface height reduction with maximum reduction (~5 cm on average) appearing at the TC center. Pre-existing COEs (AOEs) are enhanced (weakened) by TCs with an average 24% increase (17% decrease) in amplitude and enlarged (shrunk) with an average 19% increase (13% decrease) in radius. Stronger or slower-moving TCs enhance COEs more significantly. Pre-TC existing COEs (AOEs) enhance (suppress) TC-induced sea surface cooling, and thus suppress (fuel) TC intensification, with the effect of COEs statistically stronger than AOEs. This modulating effect is more pronounced under stronger or slower-moving TCs. Eddy's location also influences the modulating effect, with pre-TC COEs located to the left (right) of TC track shifting the largest cooling leftwards (rightwards). Furthermore, the left-located COEs increase cooling amplitude by 61%, stronger than right-located COEs (26%). These results suggest that the combination of mesoscale eddies and TC attributes complicates TC-induced sea surface cooling, which potentially affects TC intensification, wind structure, and rainfall.

Plain Language Summary Tropical cyclones (TCs) and mesoscale eddies, the most energetic synoptic-scale processes in the atmosphere and ocean respectively, often interact with each other at their encounters. The South China Sea (SCS) suffers the most frequent TCs among global oceans and contains active mesoscale eddies, leading to frequent TC–eddy encountering events (12.4 annually on average). Nevertheless, a systematic study on TC–eddy interaction in the SCS is lacking. Compositing 27-year satellite data, this study examines the influence of TCs on eddies and the modulation of TC-induced sea surface cooling and TC intensification by eddies over the SCS. TCs enhance cyclonic ocean eddies (COEs) and weaken anticyclonic ocean eddies (AOEs). Conversely, COEs (AOEs) enhance (suppress) TC-induced sea surface cooling and thus suppress (fuel) TC intensification. COEs located to the left of the TC track increase cooling magnitude much more than those to the right (61% vs. 26%). Rightward-located AOEs reduce cooling magnitude more than leftward-located ones (42% vs. 33%). Overall, the modulating effect of COEs is statistically stronger than AOEs, and also left COEs than right ones. These results improve our understanding of TC–eddy interaction and potentially contribute to improving forecasting of both TC intensity and eddies in the SCS.

1. Introduction

Tropical cyclones (TCs), popularly known as typhoons in the western North Pacific (WNP), feature strong winds and cyclonic wind stress (Emanuel, 1999, 2003). Under the force of strong winds, near-inertial currents are generated in the upper ocean and their shear instability triggers strong diapycnal mixing, entraining subsurface cold water into the mixed layer and resulting in significant sea surface cooling (Guan et al., 2014; Lin et al., 2003;

Niwa & Hibiya, 1997; Price, 1983; Vincent et al., 2012). The magnitude of sea surface temperature (SST) cooling can range from 1°C to 10°C (Chiang et al., 2011; Guan et al., 2021, 2024; Lin et al., 2003; Price, 1981), and the cooling often exhibits a rightward shift relative to the TC track in the Northern Hemisphere (Mei & Pasquero, 2013; Price et al., 1994; G. Wang et al., 2016). The cyclonic wind stress associated with TCs drives divergent horizontal currents in the upper ocean and induces upwelling from the thermocline, resulting in a reduction in sea surface height (Lu et al., 2020; Mei et al., 2013). In addition, it has been reported that even new cyclonic mesoscale eddies can form after TC passage (e.g., J. Li et al., 2021; L. Sun et al., 2014).

Mesoscale eddies, typically classified as cyclonic ocean eddies (COEs) and anticyclonic ocean eddies (AOEs), are ubiquitous over global oceans (Chelton et al., 2011), accounting for around 90% of upper-ocean kinetic energy (Ferrari & Wunsch, 2009). These eddies play an essential role in transporting mass, heat, salt, nutrients, and potential vorticity (Chelton et al., 2011; Dong et al., 2014; Q. Li et al., 2018; Z. Zhang et al., 2014), and can further modulate large-scale ocean circulations and climate systems (Foltz et al., 2004; Roemmich & Gilson, 2001; Y. Zhang et al., 2020). TCs and mesoscale eddies are among the most energetic synoptic-scale processes in the atmosphere and ocean, respectively. Mesoscale eddies usually propagate westwards at O (0.1 m s^{-1}), with a lifetime of O (100 days) (Chelton et al., 2011). TCs usually develop in tropical and subtropical oceans (Balaguru et al., 2016; Gray, 1968) and move much faster than mesoscale eddies (typically 5 m s^{-1}), mostly lingering over the ocean for about 5–10 days. Therefore, TCs are very likely to encounter and interact with mesoscale eddies when moving over the ocean (Ma et al., 2017).

Many previous studies have investigated the interaction between TCs and mesoscale eddies (e.g., Jaimes & Shay, 2010, 2015; S. Liu et al., 2017; Lu et al., 2016; Ma et al., 2021; Zheng et al., 2008), initially concentrating on the role of mesoscale eddies in modulating TC-induced SST cooling (Shay et al., 2000; Zheng et al., 2010) and thus TC intensification (Lloyd & Vecchi, 2011; Wu et al., 2007). Specifically, COEs (AOEs) usually enhance (suppress) SST cooling owing to sharp (weak) subsurface thermal stratification (Jaimes & Shay, 2009, 2010) and thus inhibit (favor) TC intensification (Shay et al., 2000; Walker et al., 2005). For example, when Hurricane Rita (2005) moved over the Gulf of Mexico, SST cooling of ∼1°C and ∼4°C was observed in an AOE and a COE, respectively, due to which Rita intensified to category 5 after passing the AOE and weakened to category 3 after passing the COE (Jaimes & Shay, 2009). Lin et al. (2005) reported that, when passing over a prominent AOE, Typhoon Maemi (2003) experienced rapid intensification, with its maximum wind speed increasing by 36 m s^{-1} over 36 hr. Based on a statistical study in the WNP during 2002–2011, Ma et al. (2018) revealed a significant enhancing (suppressing) effect of COEs (AOEs) on TC-induced SST cooling.

In the last decade, it has been demonstrated that TCs can exert an impact on mesoscale eddies, which was initially reported in case studies (e.g., Lu et al., 2016; L. Sun et al., 2009, 2014). For example, L. Sun et al. (2014) reported that 18 pre-existing COEs were enhanced, and even two new COEs were generated after the passage of 15 typhoons in the WNP. Lu et al. (2016) elucidated the processes that a pre-existing COE underwent when it was enhanced by Typhoon Lupit (2003) in the WNP. Using numerical experiments, Lu et al. (2020) further demonstrated that the COE enhancement was closely associated with TC-induced upwelling and potential vorticity injection. In contrast to COEs, AOEs tend to decay following the passage of TCs due to the upwelling induced by TCs. For instance, Lu et al. (2023) reported that Typhoon Kilo (2015) significantly weakened two pre-existing AOEs close to its track. In addition to case studies, Ma et al. (2021) examined and composited the impact of TCs on eddies based on TC–eddy encounters in the WNP during 2002–2017. They reported that COEs (AOEs) are enhanced (weakened) in terms of amplitude and circulation speed, and are enlarged (shrunk) in terms of radius after TC passage. They also showed that stronger or slower-moving TCs enhance COEs more significantly. The TC-induced changes in mesoscale eddies can further influence marine ecosystems, ocean circulations, and climate systems (Lin, 2012; F. Liu & Tang, 2018; L. Sun et al., 2010; Walker et al., 2014; Y. Zhang et al., 2020).

The South China Sea (SCS), which is the largest semi-enclosed marginal sea in the WNP, suffers the most frequent TCs among global oceans (Gray, 1968), with about 11 TCs passing over annually on average (Guan et al., 2018; G. Wang et al., 2007). Meanwhile, mesoscale eddies in the SCS are highly active and energetic (G. Chen et al., 2011; G. Wang et al., 2003). Furthermore, TCs and eddies in the SCS are influenced by various factors such as energetic multiscale ocean processes, the surrounding landmass, complex topography, the intrusion from the Kuroshio current, as well as their mutual interactions (Brand & Blelloch, 1974; Guan et al., 2024; Nan et al., 2015; Zhang et al., 2016). Previous studies on TC–eddy interaction in the SCS mainly focus on individual TC cases (e.g., Huang & Wang, 2022; Jin et al., 2022; Shang et al., 2015; J. Sun et al., 2023; G. Wang et al., 2009).

For instance, Jin et al. (2022) examined the modulation of SST cooling by COEs and AOEs in three typhoon cases. Huang and Wang (2022) investigated the influence of one TC case on two eddies.

Despite these previous case studies, a systematic study on TC–eddy interaction has yet to be carried out in the SCS. In this study, using 27-year satellite observations, we examined the response of sea level anomaly (SLA) and mesoscale eddies to TCs over the SCS and their dependence on TC attributes. We also investigated the modulation of TC-induced SST cooling and TC intensification by pre-existing mesoscale eddies. The present study further reveals how the relative location of eddies to the TC track influences the spatial pattern of SST cooling. The rest of the paper is organized as follows: Section 2 introduces the data and methods. Section 3 presents the results of two TC cases and composite analysis. Section 4 discusses the mechanism behind the stronger SST cooling when COEs are located to the left side of the TC track than COEs to the right side. Conclusions are summarized in Section 5.

2. Data and Methods

2.1. TC Best-Track Data Set

The TC best-track data set is obtained from the Joint Typhoon Warning Center (JTWC) (Knapp et al., 2018), which provides TC central location and maximum sustained wind speed (V_{max}) every 6 hr. The TC translation speed (Uh) is calculated by dividing the moving distance between the current location and the location 6 hr after by 6 hr. During the study period from 1993 to 2019, a total of 326 TCs passed over the study area in the SCS (10°–24°N, 105°–122°E), including TCs that originate from the WNP and TCs that generated locally in the SCS. TCs are active throughout the entire SCS but particularly active in the northern SCS (Figure 1a).

2.2. Mesoscale Eddy Data Set

Daily mesoscale eddy information is from META2.0 DT (the delayed-time version 2.0 release of the Mesoscale Eddy Trajectory Atlas Product), distributed by the Archiving, Validation, and Interpretation of Satellite Oceanographic Data (AVISO) (Chelton et al., 2011). Eddies in this data set are detected and tracked based on SLA fields (Schlax & Chelton, 2016). The eddy information has been available since 1993, consisting of eddy type (COE or AOE), position, amplitude, circulation speed, and radius. The eddy propagation speed is calculated by dividing the propagation distance of the eddy center from the current day to the next day by 24 hr Figure 1b shows the number of mesoscale eddies that pass through each 0.25° × 0.25° grid cell in the SCS during 1993–2019. The passage of an eddy is defined as occurring when the distance between the grid point and the eddy central position is equal to or smaller than the eddy radius. The eddies located in water shallower than 200 m are pre-excluded because of the high level of uncertainty linked with altimetric observations in shallow water. As reported in the literature (e.g., G. Chen et al., 2011; G. Wang et al., 2003), there are generally four eddy-active geographical regions in the SCS, that is, southwest of Taiwan Island, northwest of Luzon, southwest of Luzon, and offshore of central Vietnam.

The frequent passage of TCs and widespread distribution of eddies make TC–eddy encountering a common phenomenon in the SCS. Following the approach of Ma et al. (2021), a TC–eddy encountering event is identified when the distance between the eddy center and the TC center is equal to or smaller than the eddy radius. A total of 335 TC-eddy encountering events are identified. On average, one TC encounters at least one eddy during its lifespan. Figure 1c displays the percentage of TC track points that encounter eddies, which is higher than 30% in the western central SCS. Figure 1d displays the percentage of eddies that encounter TCs, which peaks in the northern SCS and the western central SCS. In these two regions, on average, one to two out of 10 eddies encounter TCs. Figures 1c and 1d exhibit similar spatial patterns, both suggesting that TC–eddy encounters occur most frequently in the northern SCS and the western central SCS. Both TCs and eddies are the most active in the northern SCS, leading to frequent TC-eddy encounters. What is surprising is that the probability of TC-eddy encountering is highest in the western central SCS, where eddies are relatively active while the number of TC track points is moderate. To examine the response of eddies to TCs over the SCS, we composited the eddy characteristic anomaly during TC passage, which is calculated by subtracting the pre-TC value (the average value of 15 to 11 days before TC passage).

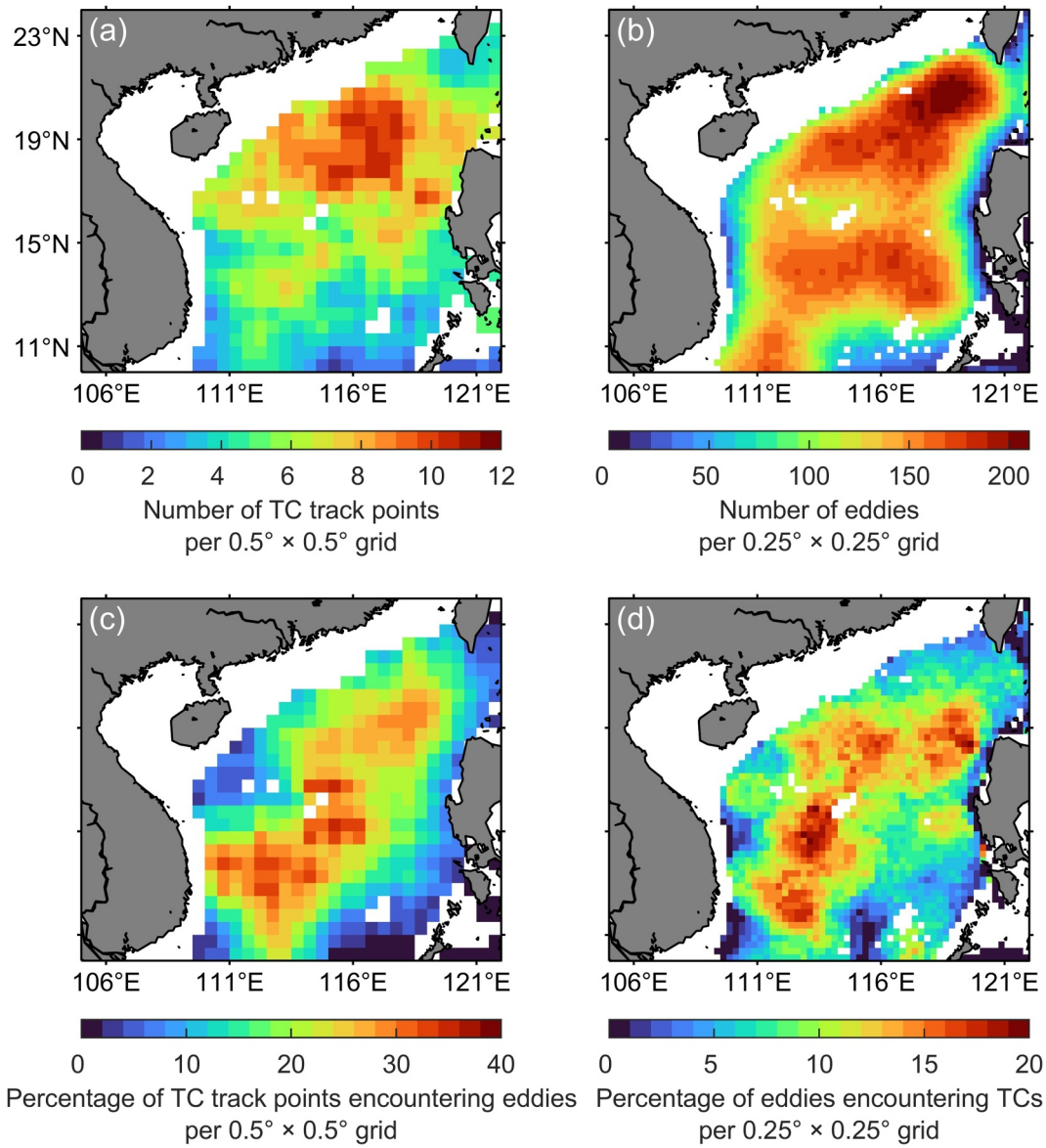

Figure 1. (a) The number of tropical cyclone (TC) track points that pass over each 0.5° × 0.5° grid cell during 1993–2019. (b) The number of mesoscale eddies that pass through each 0.25° × 0.25° grid cell during 1993–2019. (c) The percentage of TC track points that encounter eddies in each 0.5° × 0.5° grid cell. (d) The percentage of mesoscale eddies that encounter TCs in each 0.25° × 0.25° grid cell. Data in water shallower than 200 m is pre-excluded.

2.3. SLA and SST

In addition to eddy information, SLA and SST data are used to examine the sea level change and sea surface cooling induced by TCs. A daily 0.25° × 0.25° SLA data set since 1993, merged from multiple satellite missions, is obtained from the Copernicus Marine Environment Monitoring Service (CMEMS). The climatological seasonal cycle and long-term linear trend are first removed from the original SLA data at each grid point. We composited the spatial pattern of SLA change under TC-centric coordinate, following the procedure developed by Mei and Pasquero (2013). For each 6-hr TC central position, we define a domain centered on the TC center with a size of 600 km in the TC cross-track direction and 600 km in the TC along-track direction. The daily SLA data are then linearly interpolated onto the domain with a spatial resolution of 25 km × 25 km. The TC-induced SLA change is calculated by subtracting pre-TC SLA, which is defined as the average SLA of 15 to 11 days before TC passage to avoid the pre-TC SLA field being contaminated with TC-induced change (Lu et al., 2023).

The optimally interpolated (OI) SST data since 2002 (temporal resolution: daily; spatial resolution: 9 km × 9 km), derived from microwave radiometer (MW) and infrared radiometer (IR) observations (i.e., the MW + IR v5.1 product), are obtained from the Remote Sensing Systems (RSS). The climatological seasonal cycle and long-term linear trend are first removed from the original SST data. The spatial pattern of SST anomaly (SSTA) under TC-centric coordinate is also composited following the same procedure as compositing SLA change, except that the spatial resolution is 10 km × 10 km. The TC-induced SSTA is calculated by subtracting pre-TC SST (the average SST of 12 to 3 days before TC passage), following Lloyd and Vecchi (2011).

2.4. Wind Field

Wind data at 10-m height (temporal resolution: 6-hr; spatial resolution: 0.25° × 0.25°) are obtained from the ERA5 database distributed by the European Center for Medium-Range Forecasts (ECMWF) (Hersbach et al., 2023). The wind data are used to calculate Ekman pumping velocity (EPV) following Equation 1 to estimate the TC-induced upwelling.

$$\mathrm{EPV} = \frac{\nabla \times \boldsymbol{\tau}}{\rho_0 f}. \tag{1}$$

Here, ρ_0 is the seawater density, taken as 1,025 kg m^{-3}, f is the Coriolis parameter, $\boldsymbol{\tau} = \rho_a C_D \boldsymbol{U}_s |\boldsymbol{U}_s|$ is the wind stress; ρ_a is the air density, taken as 1.29 kg m^{-3}, $|\boldsymbol{U}_s|$ and $\boldsymbol{U}_s$ are 10-m wind speed and its vector, respectively; C_D, the drag coefficient, is defined as follows (Black et al., 2007; Powell et al., 2003):

$$C_D = \begin{cases} (4 - 0.6|\boldsymbol{U}_s|) \times 10^{-3} & (|\boldsymbol{U}_s| < 5 \text{ m/s}) \\ (0.7375 + 0.0525|\boldsymbol{U}_s|) \times 10^{-3} & (5 \text{ m/s} \le |\boldsymbol{U}_s| < 25 \text{ m/s}) \\ 2.05 \times 10^{-3} & (|\boldsymbol{U}_s| \ge 25 \text{ m/s}) \end{cases}. \tag{2}$$

3. Results

3.1. Case Studies: Two COEs and One AOE Affected by TCs

To detail the response of mesoscale eddies to TCs in the SCS, the generation of two COEs by TC Gaemi (2012) and the evolution of one AOE under the influence of TC Kujira (2015) are first investigated. Meanwhile, the TC-induced SST cooling is also examined in each case.

3.1.1. COEs Generated by TC Gaemi (2012)

TC Gaemi (2012) initially originated from a tropical depression in the SCS (15.4°N, 113°E) on 30 September and then moved northeastwards (Figure 2a). On 1 October, Gaemi made a sudden turn to move southeastwards and then gradually intensified until it achieved its lifetime peak intensity with a Vmax of 28 m s^{-1} on 3 October. Subsequently, Gaemi slowed down (reaching its lifetime minimum Uh of ∼1 m s^{-1}) and made its second sudden turn to move southwestwards on 4 October. After 3 days of westward motion, Gaemi made landfall in Vietnam and finally disappeared inland (not shown).

Figures 2a–2c depict the SLA evolution before, during, and after the passage of TC Gaemi. A week before Gaemi's passage, the SLA around the TC track was mostly positive (Figure 2a). As Gaemi approached, the SLA started to decrease (Figure 2b), resulting from the divergent surface flow driven by the TC's cyclonic wind stress. Two COEs (referred to as C1 and C2 here), characterized by local minimum negative SLA and cyclonic horizontal currents, were identified around the TC turning points. In the following several days, C1 and C2 continuously strengthened, and their areas increased concurrently (Figure 2c). Actually, the generation of COEs along TC track is not a rare phenomenon, as has been reported in the literature (e.g., L. Sun et al., 2010; Y. Zhang et al., 2023), especially when a TC moves slowly or makes a sudden turn, which prolongs the local residence time of wind forcing (H. Zhang et al., 2023). The generation and enhancement of the COEs can be attributed to TC-induced upwelling (Figure S1 in Supporting Information S1). As a measure of upwelling, the Ekman pumping velocity was approximately 20 and 80 m d^{-1} in C1 and C2 regions, respectively. It should be noted that the

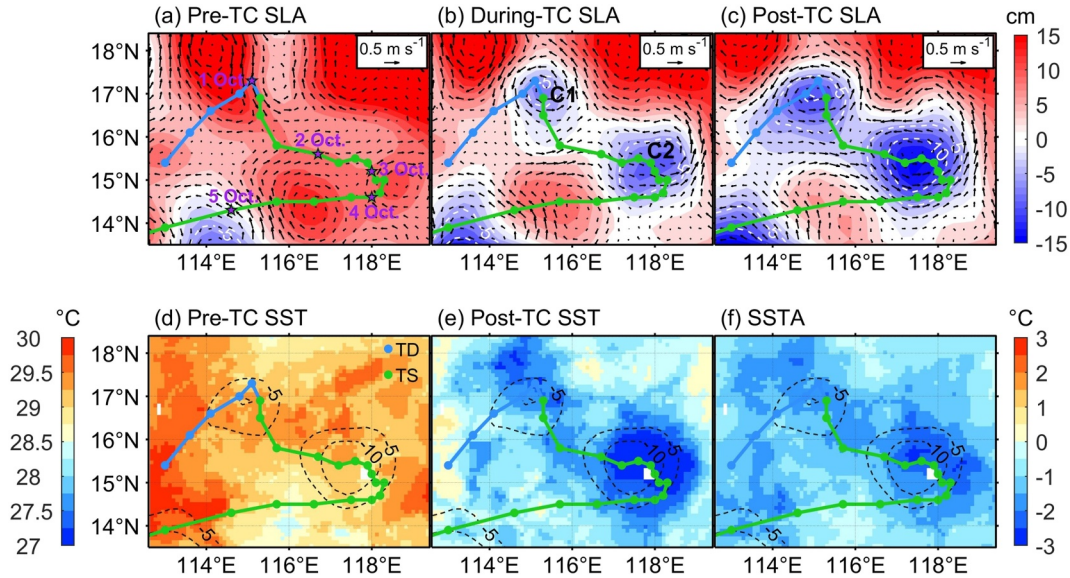

Figure 2. Ocean response to tropical cyclone (TC) Gaemi. (a–c) Sea level anomaly (SLA) evolution before (23 Sept.), during (3 Oct.), and after (10 Oct.) TC Gaemi's passage. Two COEs (named C1 and C2) are generated. Dashed white contours indicate negative SLA. Black arrows denote geostrophic currents. Colored dots and lines indicate 6-hr TC centers and the TC track, respectively. (d and e) Sea surface temperature (SST) before (26 Sept.) and after (5 Oct.) the TC passage. TC intensity categories (TD: tropical depression; TS: tropical storm) are labeled by corresponding colored dots on the upper right corner of panel (d). (f) SST anomaly (SSTA) induced by the TC, which is calculated by post-TC SST minus pre-TC SST. Dashed gray contours denote post-TC SLA.

amplitude of upwelling may be underestimated due to the coarse horizontal resolution of the ERA5 wind data set, especially under high wind conditions (Guan et al., 2014). The stronger upwelling in C2 than in C1 was because Gaemi was more intense and moved more slowly when passing over C2. Consequently, C2 was ~5 cm stronger in magnitude and ~50% larger in area than C1 (Figure 2c). As a measure of COE strength, the minimum SLA within the C2 region was reduced by more than 10 cm after Gaemi's passage (Figure 3a).

It should be noted that the SLA has begun to decrease 2 days before Gaemi's arrival (Figure 3a). This is probably because the gridded-daily SLA product used here is obtained by a temporal and spatial interpolation of sparse altimeter-based Level-3 data, the temporal and spatial resolution of which are typically larger than 10 days and 80 km (altimeter inter-track distance at the equator), respectively. Therefore, the TC-induced change is likely to have been interpolated into the pre-TC SLA field (Lu et al., 2023).

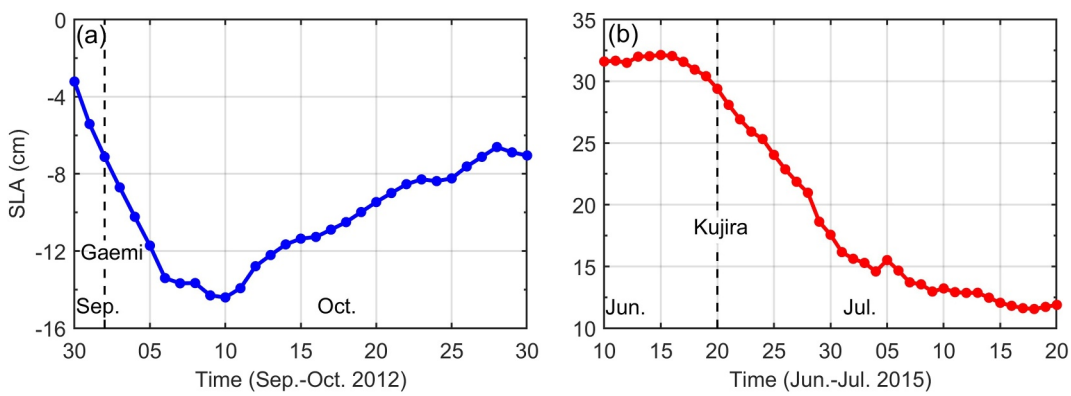

Figure 3. Time series of panel (a) minimum sea level anomaly (SLA) of C2 in Figure 2b and (b) maximum SLA of the AOE in Figure 4b. Dashed black lines in panels (a) and (b) indicate the time of Gaemi's arrival at the C2 region and Kujira's genesis in the AOE region, respectively.

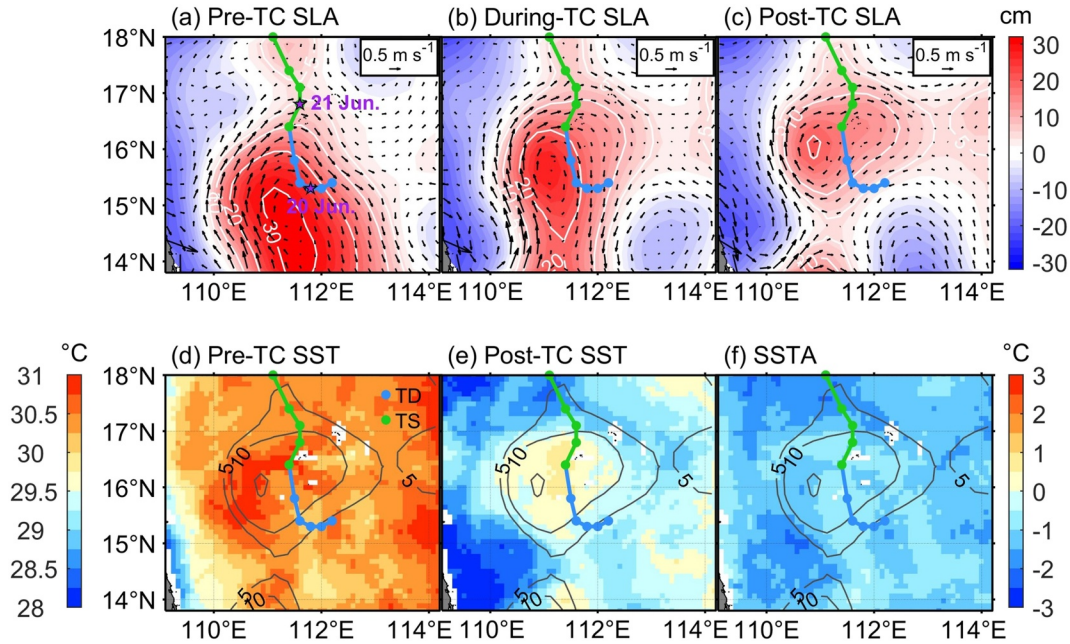

Figure 4. Ocean response to tropical cyclone (TC) Kujira. (a–c) Sea level anomaly (SLA) evolution before (10 Jun.), during (21 Jun.), and after (28 Jun.) the TC passage. Solid white contours indicate positive SLA. Black arrows denote geostrophic currents. (d and e) Sea surface temperature (SST) before (18 Jun.) and after (24 Jun.) the TC passage. TC intensity categories (TD: tropical depression; TS: tropical storm) are labeled by corresponding colored dots on the upper right corner of panel (d). (f) SST anomaly (SSTA) induced by the TC, which is calculated by post-TC SST minus pre-TC SST. Solid gray contours denote post-TC SLA.

The SST evolution during Gaemi's passage is also examined (Figures 2d–2f). Before the TC passage, the SST was generally above 29°C (Figure 2d), warmer than the minimum SST (26°C) usually required for TC development. Due to the low Uh and turning path, Gaemi's passage induced a widespread SST cooling, reducing the SST to below 28°C within a couple of days in most areas around its track (Figure 2e). Notably, two prominent cold patches (with SST of ~27°C) within the two COEs were detected after the TC passage. Especially within C2, the SST reduction ranged from 2°C to 3°C, in contrast with a reduction of generally less than 1°C outside C1 and C2 (Figure 2f). Theoretically, the TC-induced SST cooling could reduce the heat flux from ocean to atmosphere and thus inhibit TC intensification or even weaken the TC (Emanuel, 2001). The enhanced SST cooling within C2 at least partly contributed to the weakening of Gaemi, the Vmax of which dropped quickly from 28 to 18 m s^{-1} in 24 hr after passing over C2.

3.1.2. A Pre-Existing AOE Weakened by TC Kujira (2015)

TC Kujira (2015) appeared as a tropical depression in the SCS (15.4°N, 112.2°E) on 20 June and then moved westwards (Figure 4a). About 12 hr afterward, Kujira made a sudden turn to move northwards and developed into a tropical storm on 21 June. Kujira experienced continuous intensification following its genesis and achieved its lifetime peak intensity on 22 June (Vmax of 26 m s^{-1}). Subsequently, Kujira passed over Hainan Island on 22 June, then made landfall in Vietnam on 24 June, and finally disappeared inland (not shown).

Figures 4a–4c show the SLA evolution before, during, and after the passage of TC Kujira. On 10 June, a strong and large AOE existed before Kujira's genesis (Figure 4a). The maximum SLA within the AOE was maintained stably at ~32 cm (Figure 3b), suggesting a geostrophic balance state of the AOE. Kujira formed on 20 June, and lingered over the AOE for nearly 2 days, perturbing the AOE's balance state. TC's cyclonic wind stress forced a remarkable upwelling of more than 25 m d^{-1} in the AOE region (Figure S2 in Supporting Information S1), which may be underestimated due to the coarse horizontal resolution of the ERA5 wind data set. Consequently, the AOE was dramatically weakened and its size greatly decreased (Figures 4b and 4c). The maximum SLA was reduced by two-thirds of its pre-TC value, from 32 to 15 cm in 15 days (Figure 3b). Similar to the C2 case under TC Gaemi

discussed above, the commencement of the SLA reduction within the AOE was roughly 4 days earlier than Kujira's passage, which is ascribed to the interpolation of the sparse altimeter data (Lu et al., 2023).

The pre-existing AOE significantly modulated the SST cooling induced by Kujira (Figures 4d–4f). Before the TC genesis, the SST was mostly above 30°C (Figure 4d). Especially within the AOE, the pre-TC SST was ∼1°C warmer than that outside the AOE, which was conducive to the genesis of Kujira (Pun et al., 2013; Zhan et al., 2022). With the genesis and passage of Kujira, the SST experienced a continuous decline (Figure 4e). A prominent patch featuring a smaller cooling magnitude of 0.5°C–1°C than surrounding regions occupied the AOE region (Figure 4f), indicating the AOE suppressed the TC-induced SST cooling, which might help to explain Kujira's continuous intensification from its genesis until when it left the AOE.

3.2. Response of SLA and Mesoscale Eddies to TCs

Although clearly showing the influence of TCs on mesoscale eddies, the results reported in the above section are based on only two TC cases. To draw robust conclusions, we examined the SLA change and eddy characteristic anomaly induced by TCs and their dependence on TC attributes based on TCs passing over the SCS during 1993–2019.

3.2.1. Compositing TC-Induced SLA Change

The TC-induced SLA change—an important indicator of eddy evolution—is composited based on 2804 track points of 326 TCs in the SCS (Figure 5a). The TC-induced SSTA, which has been widely analyzed in previous studies (e.g., Lloyd & Vecchi, 2011; Mei & Pasquero, 2013), is also composited for comparison (Figure 5b). The SLA change and SSTA are averaged during days when their respective maximum changes occur. The SLA change is averaged on days 6–10 after TC passage (Cui et al., 2023; Mei et al., 2013), while the SSTA is averaged on days 1–3 after TC passage. Therefore, SLA change and SSTA are not simultaneous. The TC-induced SST cooling exhibits a rightward bias in the SCS (Figure 5b), consistent with previous studies (G. Wang et al., 2016; Y. Wang & Xiu, 2022). The largest SST cooling (−0.89°C) is located 40 km to the right of the TC track in the cross-track section (Figure 5c). The SLA change, however, is nearly symmetric with respect to the TC track (Figure 5a). The maximum SLA reduction (−4.67 cm) is located exactly at the TC center (Figure 5c). This discrepancy between SLA change's and SSTA's spatial pattern is mainly because TCs affect SLA and SST through different physical processes. The SST cooling is mainly induced by vertical mixing and entrainment, which are stronger on the right side of the TC track than on the left side (Price et al., 1994). The SLA reduction mainly results from the divergent Ekman flow driven by TC's cyclonic wind stress (Shay & Chang, 1997), which is roughly symmetric with respect to the TC track (Huang & Wang, 2022; Lu & Shang, 2024; Ma, 2020). Furthermore, the *e*-folding width in the cross-track section is 300 km for SLA change, narrower than that for SSTA (640 km), probably because the area of TC-induced upwelling is smaller than that of TC-induced entrainment.

The SLA change is always symmetric with respect to the TC track, regardless of TC intensity or translation speed (Uh) (Figure 6). However, the magnitude and width of the SLA change strongly depend on the two TC attributes. The maximum SLA reduction induced by strong TCs is nearly twice that induced by weak TCs (6.54 vs. 3.28 cm) (Figure 6e) since stronger winds drive stronger divergent currents. The widths of the SLA change (represented by −2 cm) induced by strong and weak TCs are 310 and 210 km, respectively, due to the fact that stronger TCs are generally larger in size (Kimball & Mulekar, 2004; Y. Liu et al., 2023). For TCs with different Uh, the maximum SLA reduction induced by slow-moving TCs is nearly three times that induced by fast-moving TCs (5.89 vs. 2.10 cm) (Figure 6f). The widths of the SLA change (represented by −2 cm) are 340 and 50 km for slow- and fast-moving TCs, respectively. Although the magnitude and width of SLA change vary, the shape of the normalized SLA change is similar across different TC intensities and Uh (Figures 6g and 6h).

The temporal evolution of the TC-induced SLA change is examined and shown in Figure 7. From 15 to ∼7 days before TC passage, the area-averaged SLA changes remain stably at approximately zero (Figure 7a), suggesting a balanced state of the ocean. From day −7, the SLA starts to rapidly decrease and drops to its lowest level approximately on day 8. The maximum SLA reduction at the TC center reaches nearly 5 cm. Subsequently, the SLA experiences a 20-day rapid exponential increase, followed by a slow increase, and recovers to approximately 1 cm lower than the pre-TC value on day 60. The recovery of SLA reduction is primarily attributed to air–ocean heat flux via thermal expansion of water as well as geostrophic adjustment and westward propagation associated

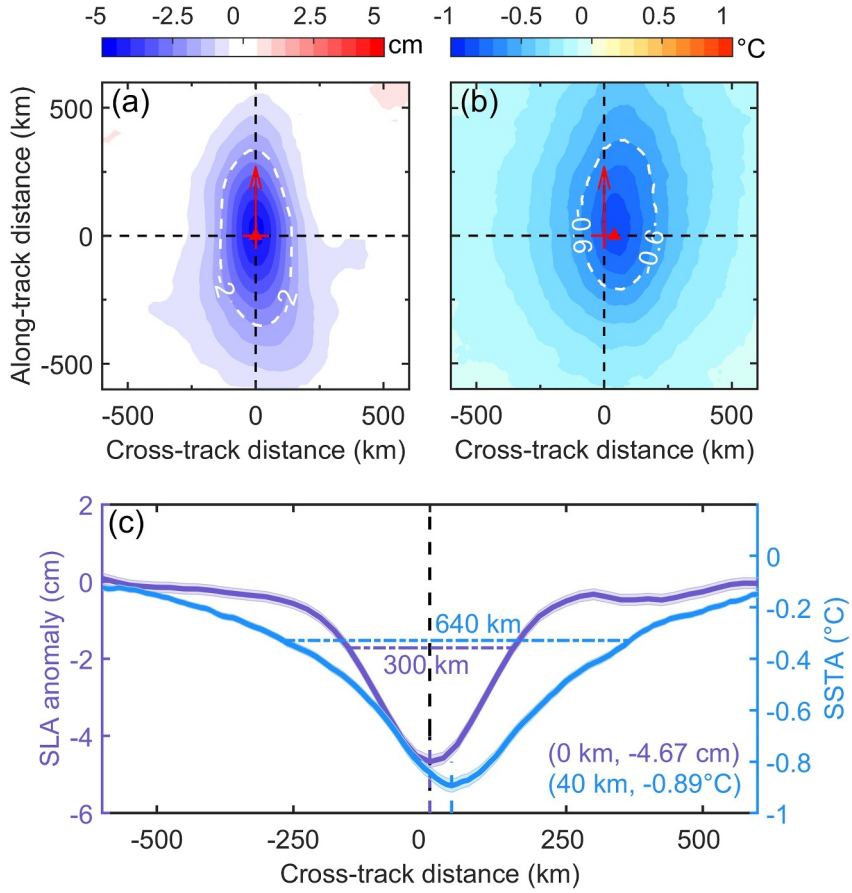

Figure 5. Spatial pattern of composited (a) sea level anomaly (SLA) change and (b) sea surface temperature anomaly (SSTA) induced by tropical cyclones (TCs). Red crosses denote the TC center and red arrows denote TC moving direction. Red solid triangles in panels (a) and (b) represent the locations of maximum SLA and SST reduction in the cross-track section, respectively. (c) SLA change and SSTA in the across TC track section. Horizontal dash-dotted lines indicate the widths of SLA change (SSTA) being e^{-1} times the minimum SLA change (SSTA). Shaded error bars represent standard errors.

with eddies (Mei et al., 2013). The westward propagation speed of the SLA change is ~0.1° d^{-1} (Figure 7c), consistent with the result in the open ocean (Cushman-Roisin et al., 1990; Jansen et al., 2010). The *e*-folding recovery time (Γ) of the normalized SLA change is ~24 days, estimated based on a nonlinear least squares fit to an exponential curve following Equation 3 by Mei and Pasquero (2013), which reveals that the recovery time of TC-induced SSTA is approximately 10 days.

$$\mathrm{SLA}(t) = A\exp\left(-\frac{t}{\Gamma}\right). \tag{3}$$

Although the magnitude of area-averaged SLA change decreases with the area increasing (Figure 7a), the temporal evolution of area-averaged SLA changes within different-size areas is similar, which is more clearly presented by the normalized SLA change (Figure 7b). Interestingly, the timing of area-averaged SLA reaching maximum reduction lags with the area increasing, probably because the average SLA within a larger area involves SLA change induced by following several TC track points.

As mentioned in Section 3.1, the decrease in SLA starts from day −7 instead of day 0, mainly because the interpolation of altimeter data maps the TC-induced SLA change onto pre-TC SLA field, as discussed in detail by Lu et al. (2023). Similarly, the pre-TC SLA field could also be mapped onto post-TC SLA field during the interpolation. Furthermore, the chance that altimeters accurately capture maximum SLA reduction is slight, owing to the long sampling period of altimeters. In addition, the rainfall concurrent with TC passage also interferes with the altimeter-observed SLA (Carrère et al., 2009). Given these uncertainties, the TC-induced SLA

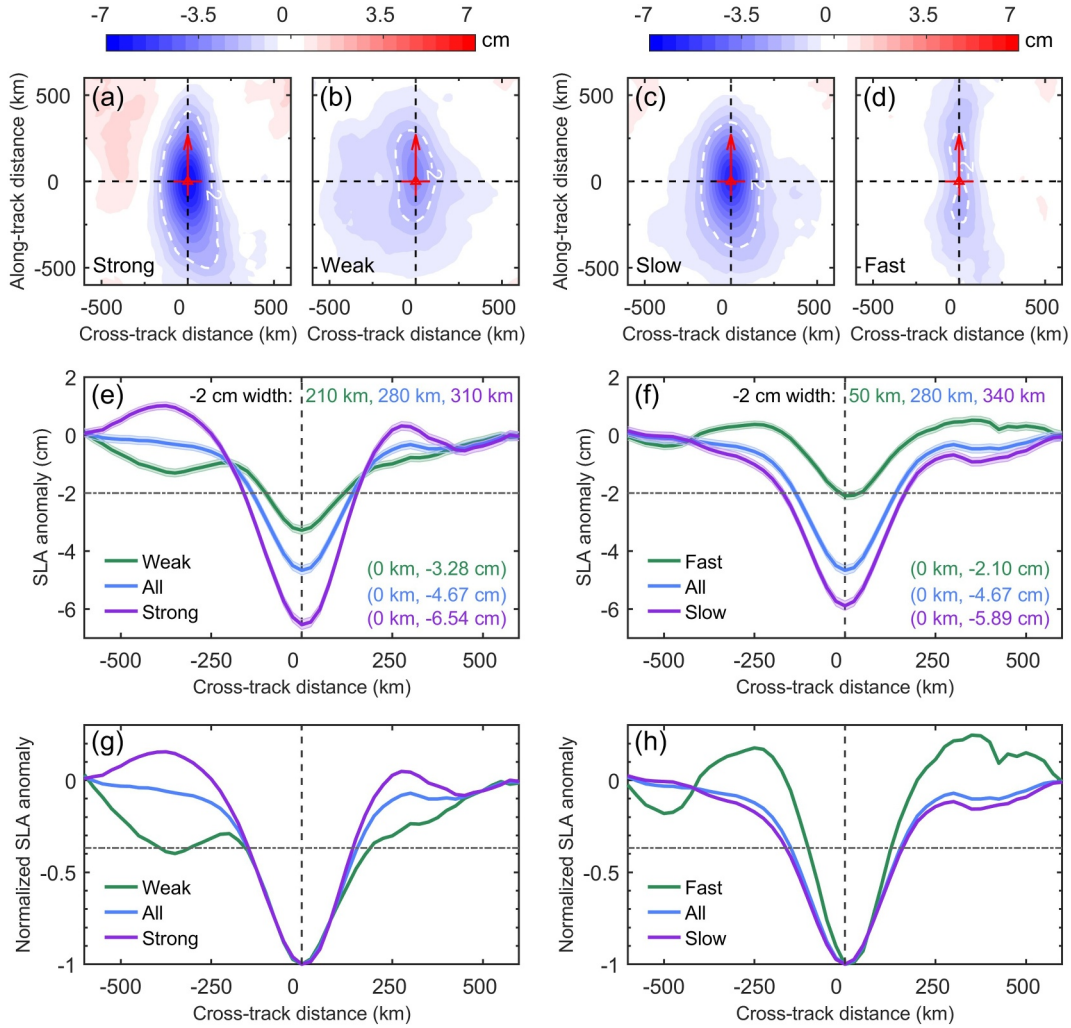

Figure 6. Spatial pattern of composited sea surface anomaly (SLA) change induced by tropical cyclones (TCs) with (a) maximum wind speed (V_{max}) ≥ 21 m s^{-1} (strong), (b) V_{max} < 21 m s^{-1} (weak), (c) translation speed (Uh) < 5 m s^{-1} (slow), and (d) Uh ≥ 5 m s^{-1} (fast). (e) The SLA change in the across TC track section for strong, all, and weak TCs. The horizontal gray dash-dotted line indicates SLA change = −2 cm. Shaded error bars represent standard errors. (f) As in panel (e) but for fast, all, and slow TCs. (g) and (h) As in panels (e) and (f) but for the SLA change normalized by dividing their respective maximum SLA reduction. The horizontal gray dash-dotted line indicates the normalized SLA change = $-e^{-1}$.

reduction is likely to be underestimated based on altimeter data, and the observed timing of maximum SLA reduction after TC passage may not be perfectly exact.

3.2.2. Response of COEs and AOEs to TCs

Although the TC-induced SLA reduction to some extent represents mesoscale eddy changes (Jansen et al., 2010), we cannot detail the influence of TCs on COEs and AOEs directly from the SLA change. Using the mesoscale eddy data set derived from SLA fields (Chelton et al., 2011), we composited the eddy characteristic anomaly based on a total of 335 TC–eddy encountering events over the SCS during 1993–2019, including 183 TC–COE and 152 TC–AOE encountering events. The TC–eddy encountering is identified when the distance between the eddy center and the TC center is equal to or smaller than the eddy radius (Ma et al., 2021), which is reasonable since the average eddy radius in the SCS is 130 km (G. Chen et al., 2011), and the TC-induced SLA change is pronounced within 150 km from the TC center (Figure 6).

Figure 8 shows the temporal evolution of eddy characteristic anomaly before and after TC passage. The evolutions of amplitude and circulation speed exhibit highly similar features since both are indicators of eddy strength

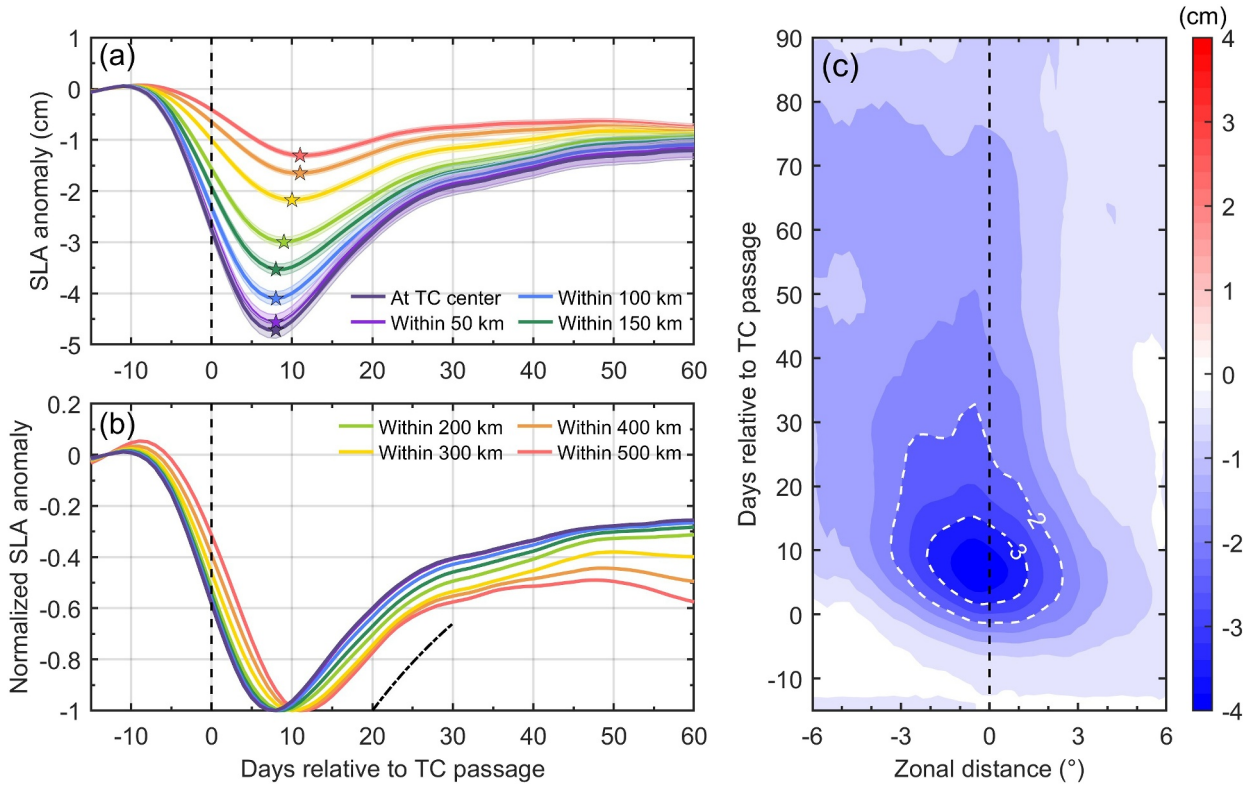

Figure 7. (a) Time series of composited sea level anomaly (SLA) change at the tropical cyclone (TC) center and area-averaged SLA change within 50–500 km around the TC center. Pentagram denotes maximum SLA reduction. Shaded error bars represent standard errors. (b) As in panel (a) but for the SLA change normalized by dividing their respective maximum SLA reduction. The black dash-dotted line indicates an exponential function with an *e*-folding time of 24 days. (c) Hovmöller diagram showing the composited SLA change in the zonal section centered on the TC track for TCs moving within 45° of the poleward direction.

(Figures 8a and 8c). For COEs, before TC passage, the amplitude and circulation speed remain stable, suggesting a balanced state. As TCs approach, the amplitude and circulation speed begin to increase, reaching their peaks at roughly day 21, with an increase of ∼2 and ∼2.5 cm s^{-1}, representing a 24% and 8% increase from pre-TC values (8.2 and 30.5 cm s^{-1}), respectively. Following the peak, the amplitude and circulation speed rapidly decrease, recovering to pre-TC values on day 37 and day 32 (not shown here), respectively. For AOEs, the amplitude and circulation speed also remain stable before TC passage and subsequently decrease by ∼1.5 and ∼2.5 cm s^{-1}, representing a 17% and 8% reduction from pre-TC values (8.9 and 30.1 cm s^{-1}), respectively. The reduction is followed by an increase from day 19. It should be noted that the observed enhancement of COEs and weakening of AOEs start from approximately day −7, instead of the arrival time of TCs, which is attributed to the interpolation of altimeter data (Lu et al., 2023).

After TC passage, the COE radius is raised by ∼20 km, 19% of the pre-TC value, while the AOE radius is reduced by ∼15 km, 13% of the pre-TC value (Figure 8b). As for the eddy propagation speed, generally, COEs propagate more slowly, while AOEs propagate more quickly after TCs than before (Figure 8d), since weaker eddies are more likely to flow with background currents. Overall, the statistical response of mesoscale eddies to TCs over the SCS is generally consistent with that in the WNP (Ma et al., 2021), although both TCs and eddies in the SCS, a marginal sea, are also influenced by many other factors, such as the complex topography (Z. Zhang et al., 2016).

We then examined the dependence of the eddy response on TC intensity (V_{max}) and Uh using maximum eddy characteristic anomaly, which is defined as the first local maximum (minimum) characteristic anomaly during days 0–30 for COEs (AOEs) (Figure 9). For COEs, the magnitude of amplitude (circulation speed) anomaly roughly increases monotonically as the Vmax increases or Uh decreases (Figures 9a–9d). For instance, the amplitude (circulation speed) anomaly associated with Vmax larger than 29 m s^{-1} and smaller than 13 m s^{-1} is 3.1 cm (5.1 cm s^{-1}) and 1.1 cm (0.8 cm s^{-1}), respectively. The amplitude (circulation speed) anomaly associated with Uh lower than 3 m s^{-1} and higher than 7 m s^{-1} is 3.9 cm (6.2 cm s^{-1}) and 0.2 cm (0.4 cm s^{-1}), respectively.

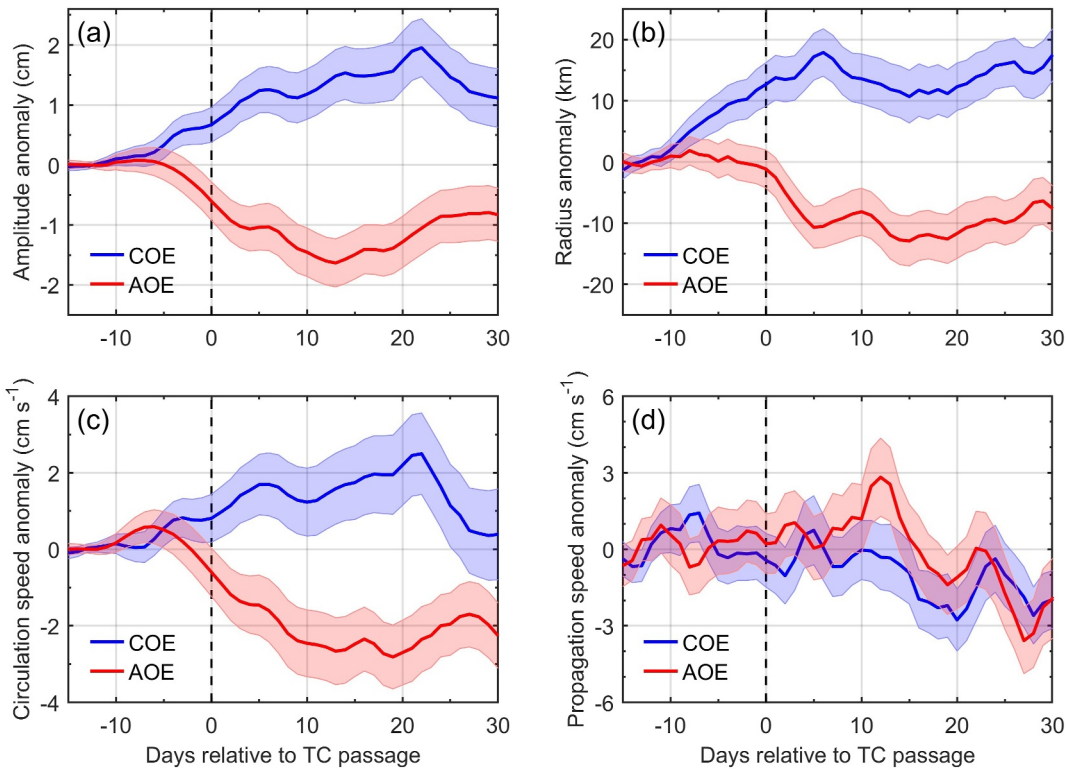

Figure 8. Time series of mesoscale eddy characteristic anomaly including (a) amplitude anomaly, (b) radius anomaly, (c) circulation speed anomaly, and (d) propagation speed anomaly, for cyclonic ocean eddies (COEs) and anticyclonic ocean eddies (AOEs). Shaded error bars represent daily standard errors. A 3-day running mean smoothing is applied.

The dependence of COE radius anomaly on the Vmax or Uh is also roughly monotonic (Figures 9e and 9f), although not as pronounced as that of the COE amplitude anomaly. Interestingly, the variation of AOE characteristic anomaly with the Vmax or Uh is not monotonic and could not be recognized well, but the results still indicate that roughly strong or slow-moving TCs tend to weaken and shrink AOEs greatly (Figure 9).

Overall, TCs strongly influence the evolution of mesoscale eddies over the SCS in terms of eddy strength, radius, and propagation speed. Specifically, COEs are enhanced and enlarged after TC passage (Figure 8), and this response is more pronounced when TCs are stronger or slower-moving (Figure 9). By contrast, AOEs are weakened and shrunk (Figure 8), but this response is not as sensitive to TC intensity and Uh as the COE response (Figure 9).

3.3. Modulation of SST Cooling and TC Intensification by COEs and AOEs

In the TC–ocean coupled system, not only can TCs significantly affect the evolution of mesoscale eddies, but pre-existing eddies can also modulate TC-induced SST cooling and further feedback onto TC intensification, which we examined next based on 198 TCs that passed over the SCS during 2002–2019. A total of 1578 TC track points are involved here, including 227 track points within COE regions and 141 within AOE regions. We composited the spatial pattern of TC-induced SSTA when pre-TC existing COE or AOE is located to the left or right of the TC track (hereafter referred to as left-COE, right-COE, left-AOE, or right-AOE conditions) and when there is no pre-existing eddy (COM condition) for comparison (Figure 10). The SSTA is averaged on days 1–3 after TC passage.

Compared with COM conditions, pre-existing COEs enhance TC-induced SST cooling on both sides of the TC track, as shown in Figures 10a–10c. The maximum cooling enhancement is located on the left and right sides of the TC track under left- and right-COE conditions, respectively (Figure 10h). Consequently, their respective locations of the largest cooling shift leftwards and rightwards compared with COM condition but are still rightward-biased, appearing at 10 km, 70 km, and 40 km to the right of the TC track under left-COE, right-COE, and COM conditions, respectively (Figure 10f). SST cooling under left-COE condition is stronger than that under

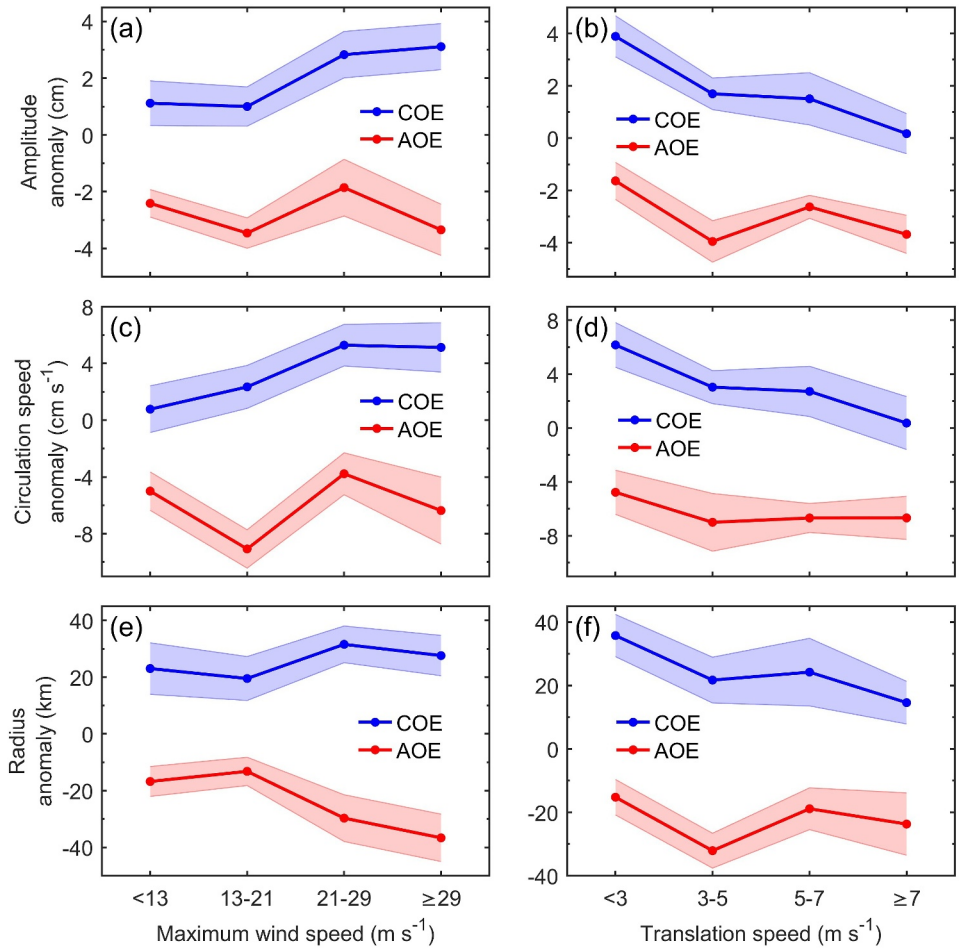

Figure 9. (a) and (b) Maximum amplitude anomaly, (c) and (d) maximum circulation speed anomaly, (e) and (f) maximum radius anomaly as functions of panels (a, c, and e) TC maximum wind speed and (b, d, and f) TC translation speed, for cyclonic ocean eddies (COEs) and anticyclonic ocean eddies (AOEs). Shaded error bars represent standard errors.

right-COE condition; their respective maximum cooling magnitudes in the cross-track section are 1.42°C and 1.11°C, representing an increase of 61% and 26% compared with COM condition (0.88°C), respectively (Figure 10f; Table 1). The width of SST cooling is further estimated by the SSTA = −0.6°C contour. Under COM, left-COE, and right-COE conditions, the respective widths of SST cooling are 280, 430, and 300 km, indicating that COEs enlarge the cooling area, and this effect seems more pronounced by left COEs than by right COEs.

In contrast, pre-existing AOEs suppress the TC-induced SST cooling, as shown in Figures 10c–10e. Compared with COM condition, the largest cooling is suppressed by 33% (42%) under left-AOE (right-AOE) condition, appearing at 100 km (30 km) to the right of the TC track (Figure 10g; Table 1). Additionally, AOEs reduce the cooling area, as indicated by the widths of −0.4°C SSTA, which are 530, 370, and 290 km under COM, left-AOE, and right-AOE conditions, respectively. Overall, the suppression of cooling by right AOEs is slightly stronger than that by left AOEs in the SCS.

Given the fact that TC-induced SST cooling is also influenced by TC attributes (Mei & Pasquero, 2013; Y. Wang, 2020), we further examined the modulation of the SSTA by COEs and AOEs as a function of TC intensity (V_{max}) and translation speed (Uh) (Figure 11). The SSTA magnitude increases with the Vmax increasing or Uh decreasing, consistent with previous studies (e.g., Ma et al., 2018; Mei & Pasquero, 2013; Y. Wang & Xiu, 2022). Under TCs of the same Vmax or Uh range, the SSTA magnitude under COE condition is mostly larger than that under COM condition. Furthermore, this difference increases with the Vmax increasing or Uh decreasing. For example, the SSTA difference between COE and COM conditions is about 0.01°C when Vmax is lower than 13 m s^{-1} but reaches 0.7°C when Vmax is higher than 29 m s^{-1} (Figure 11a). The SSTA amplitude under COE

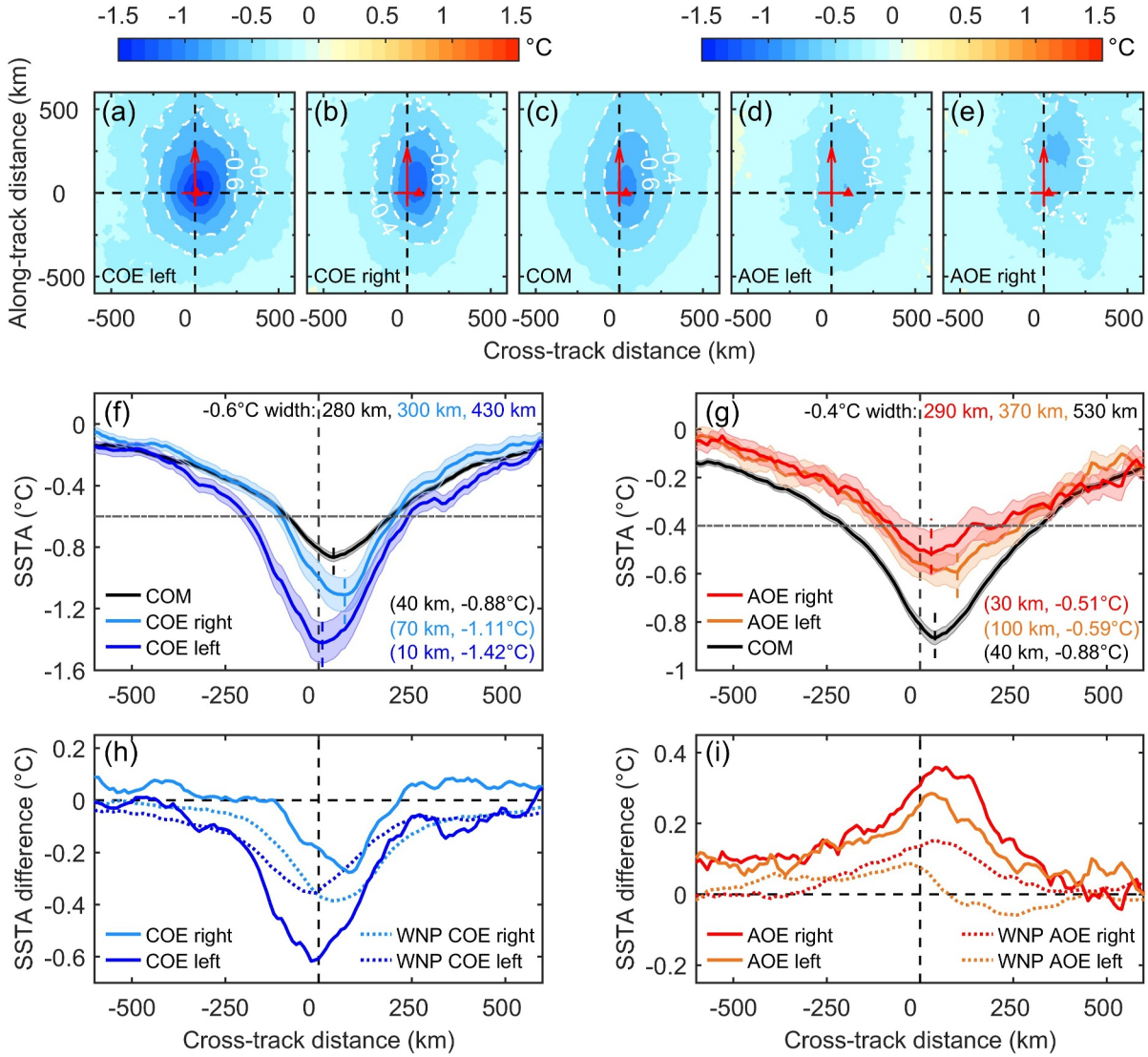

Figure 10. Spatial pattern of composited tropical cyclone-induced (TC-induced) sea surface temperature anomaly (SSTA) under (a) left-COE (relative to the TC track), (b) right-COE, (c) COM, (d) left-AOE, and (e) right-AOE conditions. Red solid triangles denote minimum SSTA in the across TC track section. (f) The TC-induced SSTA in the across TC section under COM, right-COE, and left-COE conditions. The horizontal dash-dotted gray line indicates SSTA = −0.6°C. Shaded error bars represent standard errors. (g) As in panel (f) but under right-AOE, left-AOE, and COM conditions. The horizontal dash-dotted gray line indicates SSTA = −0.4°C. (h) and (i) The SSTA difference with respect to the SSTA under COM condition in the cross-track section. Solid and dotted lines indicate values in the South China Sea and western North Pacific (WNP), respectively.

condition is 0.5°C and 0.2°C larger than that under COM condition for Uh lower than 3 m s^{-1} and higher than 7 m s^{-1}, respectively (Figure 11b). In contrast to COEs, the SSTA magnitude under AOE condition is mostly smaller than that under COM condition, and the SSTA difference between the two conditions also exhibits an increase as TCs intensify or slow down. Overall, the enhancing (suppressing) effect of COEs (AOEs) on SST cooling is more pronounced for stronger or slower-moving TCs.

Table 1
The Magnitude and Location of the Largest Sea Surface Temperature (SST) Cooling in the Across Tropcial Cyclone (TC) Track Section

Largest SST cooling	COE left	COE right	COM	AOE left	AOE right
Magnitude (°C)	1.42	1.11	0.88	0.59	0.51
Location (km)	+10	+70	+40	+100	+30

Note. The positive value of the location means that the location is on the right side of the TC track.

At the TC center, the SSTA magnitude within COEs is 49% higher than that under COM condition, above the 95% confidence level, while the SSTA magnitude is reduced by 39% within AOEs, above the 95% confidence level (Figure 12a). The modulating effect on SST cooling is more pronounced by strong COEs (−1.35°C) than weak COEs (−0.96°C), while the dependence of the modulating effect on AOE strength is weak (−0.47°C for strong AOEs vs.

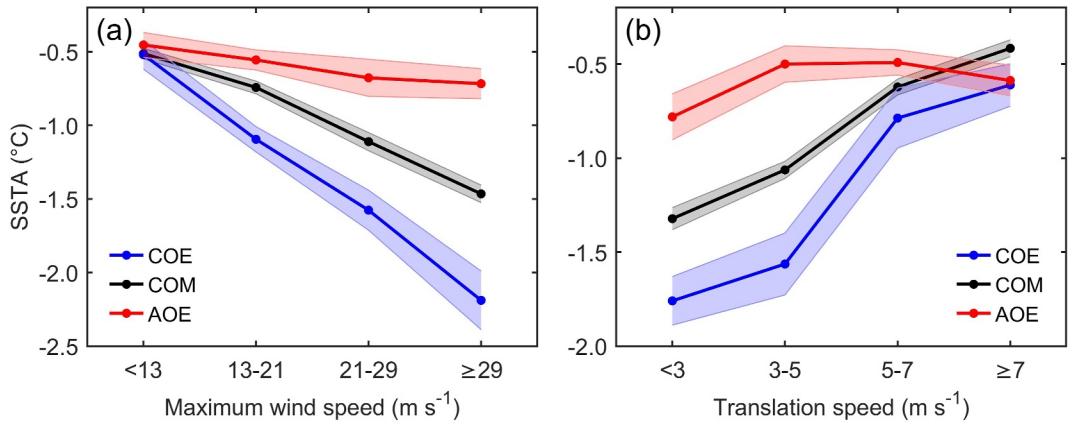

Figure 11. The sea surface temperature anomaly (SSTA) at the tropical cyclone (TC) center as a function of TC (a) maximum wind speed and (b) translation speed under COE, COM, and AOE conditions. Shaded error bars represent standard errors.

−0.48°C for weak AOEs). The modulated SST cooling is expected to further feedback onto TC intensity. As a measure of TC intensity change, the TC intensification rate is defined as the Vmax change in the subsequent 24 hr after passing the current location. On average, the TC intensification rate under COE condition is 0.54 m s^{-1} per 24 hr (47%) lower than that under COM condition, above the 95% confidence level (Figure 12b). Under AOE condition, the TC intensification rate is raised by 0.14 m s^{-1} per 24 hr (12%), although not as significantly as the change within COEs. A possible explanation is that the effect of AOEs on TC intensification also depends on the distance between the AOE and the TC center. If an AOE is located far away from the TC center, TC intensification is inhibited because the AOE weakens the TC secondary circulation and reduces the energy conversion from the ocean to the TC, as proposed by J. Sun et al. (2023).

4. Discussion

An unexpected result in the SCS is that the TC-induced SST cooling is stronger when COEs are located to the left side of the TC track than when COEs to the right side, while the phenomenon is not found in the WNP (Figure 10). To uncover the underlying mechanism behind this phenomenon, we examined factors that affect TC-induced SST cooling, including eddy amplitude, TC intensity, storm size, TC translation speed (Uh), and climatological ocean thermal stratification over which COEs are overlaid. The average eddy amplitude of left COEs is smaller than that of right COEs (9.2 vs. 9.7 cm), which cannot explain stronger SST cooling under left-COE condition, as weaker

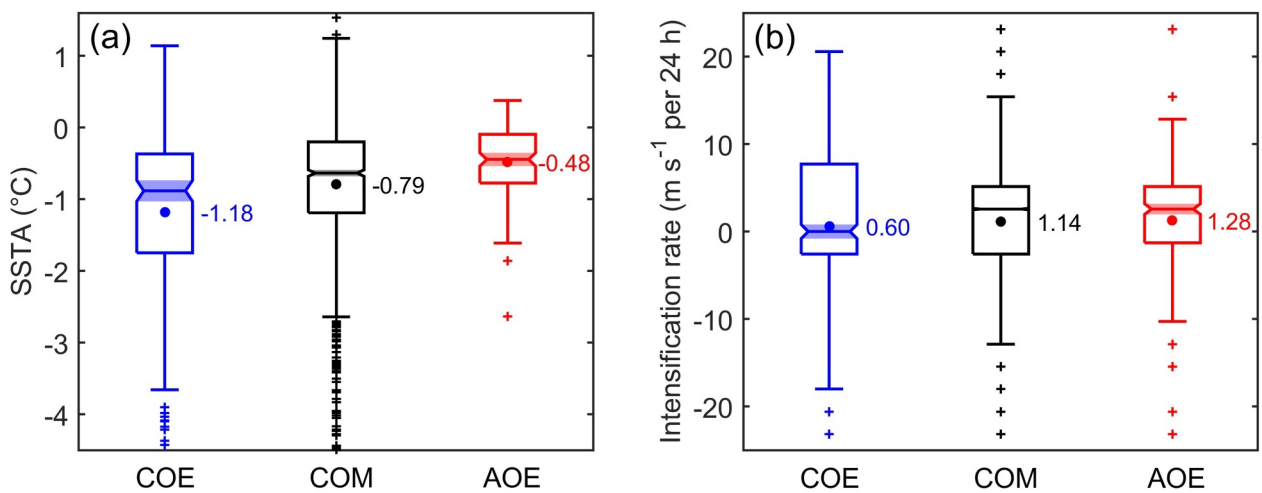

Figure 12. Boxplots of panel (a) sea surface temperature anomaly (SSTA) at the tropical cyclone (TC) center and (b) TC intensification rate under COE, COM, and AOE conditions. The solid dot in each box denotes the average value, which is texted on the right of the corresponding box. The middle line of each box indicates the median. The shaded region of each box is called the notch and two boxes with nonoverlapping notches have different medians above the 95% confidence level.

Table 2
Settings in Different Experiments

Experiments	Translation speed of tropical cyclone (TC)	Initial ocean temperature	Position of cyclonic ocean eddy (COE) center
Exp_Cr	4.3 m s^{-1}	Profile 1	+80 km
Exp_Cl	4.3 m s^{-1}	Profile 1	−80 km
Exp_Cl_T	4.3 m s^{-1}	Profile 2	−80 km
Exp_Cl_T_Uh	3.5 m s^{-1}	Profile 2	−80 km

Note. The initial ocean temperature profile is the profile before incorporating eddy-induced isotherm displacements. Profile 1 and Profile 2 denote the composited temperature profile within 300 km of the TC center under right-COE and left-COE conditions, respectively (Figure S3 in Supporting Information S1). COE center is positioned in the section across the midpoint of *y* axis. "+80 km" and "−80 km" mean that the COE center is located 80 km to the right and left of the TC track, respectively.

COEs are expected to enhance SST cooling to a lesser extent. The maximum wind speeds of TCs encountering left and right COEs are both approximately 25 m s^{-1}, which also cannot account for the stronger cooling enhancement under left-COE condition. The storm sizes, in terms of 34-kt wind radii, are 152 and 185 km for TCs encountering left and right COEs, respectively. As smaller TCs tend to generate weaker SST cooling (Y. Liu et al., 2023), smaller storm size also cannot explain stronger SST cooling under left-COE condition. Nevertheless, we find that the average TC Uh under left-COE condition (3.5 ± 0.4 m s^{-1}) is significantly lower than that under right-COE condition (4.3 ± 0.3 m s^{-1}), above the 95% confidence level, while TC Uh in the WNP shows no significant difference between left- and right-COE conditions. The background thermal stratification over which COEs are overlaid may also influence the cooling enhancement. Using climatological monthly temperature data from World Ocean Atlas 2018, we extracted ocean temperature profiles along the TC cross-track section and averaged them within 300 km of the TC center for each TC track point. The composited temperature profile for TCs encountering left COEs shows sharper thermal stratification in the upper 50 m than that for TCs encountering right COEs (Figure S3 in Supporting Information S1), probably due to different distributions of latitudes where TCs encounter left or right COEs. Therefore, the TC Uh and climatological ocean thermal structure are two candidates responsible for the stronger cooling under left-COE condition.

To further confirm and quantify the relative contributions from Uh and thermal stratification, we conducted numerical experiments by employing the three-dimensional Price-Weller-Pinkel model (3DPWP; Price et al., 1994), which has been widely used in TC-ocean interaction studies (e.g., Balaguru et al., 2015; Guan et al., 2014; Lin et al., 2013; Pun et al., 2018; Walker et al., 2014; Ye et al., 2023; Y. Zhang et al., 2023). The 3DPWP model used in this study is a newly modified version, which can include a geostrophic eddy by incorporating isotherm displacements and geostrophic currents associated with the eddy into the initial field. In this study, the model is configured with horizontal grids at resolutions of 5 km × 5 km and the domain size is 1,000 km × 1,000 km. In the vertical direction, the domain extends to a depth of 1,000 m and is divided into 45 layers, with a 5-m interval of the first 20 layers, a 10-m interval of the middle 10 layers, and a 50-m interval of the last 15 layers. The time step is 600 s. The f-plane is utilized with the latitude set at 16°N, which is the average latitude of TC track points encountering COEs.

Four experiments are designed (Table 2). In the control experiment (Exp_Cr), TC moves at a constant speed of 4.3 m s^{-1}; the background ocean temperature before incorporating eddy-related isotherm displacements is the composited climatological temperature profile for TCs encountering right COEs (Figure S3 in Supporting Information S1); a COE is placed 80 km to the right of the TC track (Figure 13a; Figure S4b in Supporting Information S1). The second experiment (Exp_Cl) setting is the same as experiment Exp_Cr but a COE is placed 80 km to the left of the TC track (Figure 13b; Figure S4c in Supporting Information S1). The third experiment (Exp_Cl_T) setting is the same as experiment Exp_Cl but the background ocean temperature before incorporating eddy-related isotherm displacements is the composited climatological temperature profile for TCs encountering left COEs (Figure S3 in Supporting Information S1). The fourth experiment (Exp_Cl_T_Uh) setting is the same as experiment Exp_Cl_T but for the TC Uh of 3.5 m s^{-1}.

In each experiment, TC moves along the *y*-axis from the center of the bottom edge with maximum wind speed of 25 m s^{-1}. The wind pattern of TCs is based on the idealized Rankine vortex, with the radius of maximum wind speed being 50 km (Figure S4a in Supporting Information S1). For the COE, the radius is 130 km and the

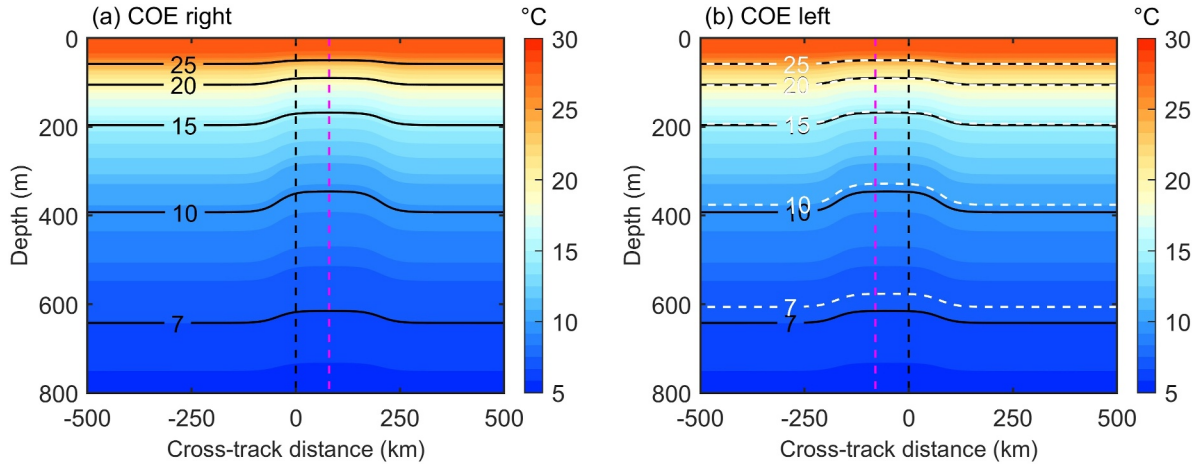

Figure 13. Initial vertical temperature section across tropical cyclone (TC) track in panel (a) experiment Exp_Cr and (b) experiment Exp_Cl. The dashed white lines in panel (b) indicate the temperature profile in experiments Exp_Cl_T and Exp_Cl_T_Uh. The vertical dashed black and magenta lines denote the positions of the TC track and eddy center, respectively.

maximum isotherm displacement is 50 m at 300 m depth. The center of COE is positioned in the section across the midpoint of the *y*-axis. The initial current is the superposition of static current and geostrophic current associated with the COE (Figure S4 in Supporting Information S1).

Figure 14 shows the simulated cross-track SSTA and SSTA difference with respect to experiment Exp_Cr. The SSTA is calculated by subtracting the initial SST from the average SST during days 1–3 after TC passage. SST cooling in all experiments is rightward-biased. The largest SST cooling in experiments Exp_Cr and Exp_Cl_T_Uh is −1.13°C and −1.38°C, respectively, which are roughly consistent with the composited SSTA using satellite observations (Figure 10f). Furthermore, the SST cooling on both sides of the TC track is stronger in experiment Exp_Cl_T_Uh than in experiment Exp_Cr (Figure 14). However, under the same TC Uh and background climatological ocean thermal stratification, the largest cooling under left-COE condition (experiment Exp_Cl) is smaller than that under right-COE condition (experiment Exp_Cr), as is the SST cooling on the right side of the TC track. Taking the largest cooling as a metric, the cooling amplitude in experiment Exp_Cl_T_Uh is 0.30°C larger than that in experiment Exp_Cl. The contribution to the difference from slow TC Uh and ocean thermal stratification is 77% and 23%, respectively. We further explored the potential effect of slow Uh and thermal stratification on SST cooling under right-COE condition by designing additional experiments assuming that the right COE experiment also operated under slow Uh (3.5 m s^{-1}) and utilized Profile 2 as the initial thermal stratification (Figure S5 in Supporting Information S1). Results show that with the same Uh and thermal stratification, SST cooling under right-COE condition (experiment Exp_Cr_T_Uh) would be comparable to that under left-COE condition (experiment Exp_Cl_T_Uh). Therefore, the stronger SST cooling enhancement under left-COE condition than

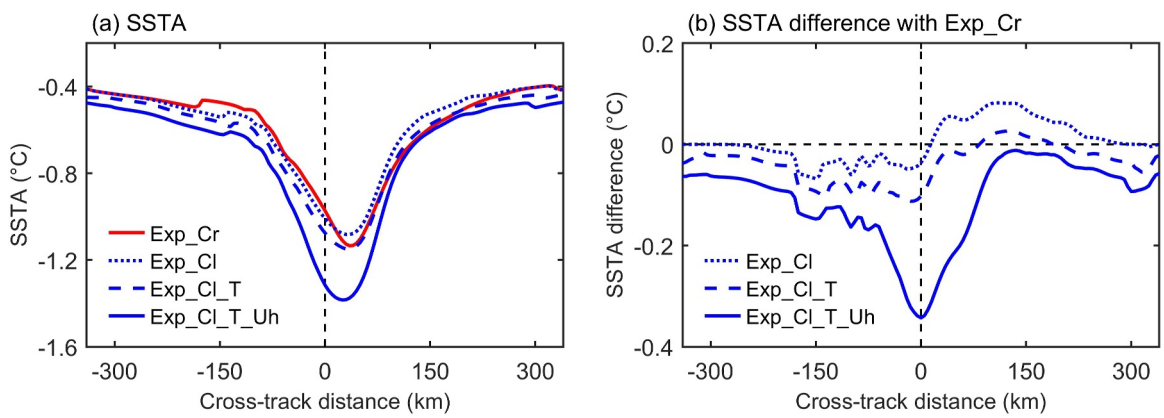

Figure 14. (a) Simulated sea surface temperature anomaly (SSTA) in four experiments. (b) Simulated SSTA difference with respect to experiment Exp_Cr.

right-COE condition in the SCS (Figure 10) is primarily attributed to the combined effect of slow TC Uh and relatively sharp background thermal stratification over which COEs are overlaid. The results suggest that the combination of mesoscale eddies, climatological ocean thermal stratification, and TC attributes (such as Uh here) further complicates the magnitudes and spatial patterns of TC-induced SST cooling. This will in turn influence TC intensification, wind structure, and rainfall, as well as the heat uptake into the subsurface ocean by TCs (D. Y.-C.F Chen et al., 2011; Ye et al., 2023).

5. Conclusions

TCs and mesoscale eddies are energetic mesoscale processes in the atmosphere and ocean, respectively. Encounters and interactions between TCs and eddies frequently occur and are one of the present hotspots, stimulating many studies in recent years (e.g., Jaimes & Shay, 2009, 2010; Lin, 2012; S. Liu et al., 2017; Lu et al., 2016, 2020; Ma et al., 2018, 2021; L. Sun et al., 2010, 2014; Walker et al., 2014; Y. Zhang et al., 2020). As the largest semi-enclosed marginal sea in the WNP, the SCS not only suffers highly frequent TCs but also contains active mesoscale eddies, serving as a perfect ocean basin for studying TC–eddy interaction. However, a systematic study on TC–eddy interaction over the SCS is still lacking. Using 27-year satellite data, we identified 183 TC-COE encountering events and 152 TC-AOE encountering events in the SCS. We found that TC-eddy encountering events are mainly concentrated in the northern SCS and the western central SCS, where one to two out of 10 eddies encounter TCs. On average, one TC encounters at least one eddy during its lifespan in the SCS. We then investigated the response of mesoscale eddies to TCs and the modulation of TC-induced SST cooling and TC intensification by pre-existing eddies.

We first detailed the evolution of two COEs and one AOE after encountering TCs. Two COEs were generated and then enhanced and enlarged owing to TC Gaemi's (2012) passage. Meanwhile, the TC-induced SST cooling within the COE region was enhanced. TC Kujira (2015) formed over a pre-existing AOE region and lingered over the AOE for 2 days, leading to a dramatic reduction in the strength and size of the AOE. In contrast with the COEs, the TC-induced SST cooling within the AOE region was suppressed.

TC-induced SLA change is an important indicator of eddy evolution, and thus we first composited SLA change induced by TCs. TCs induce a symmetric SLA reduction with maximum reduction appearing at the TC center, regardless of TC intensity and Uh. Stronger or slower-moving TCs induce more pronounced SLA reduction both in magnitude and width, while the shape of the normalized SLA change is similar across different TC intensities and Uh. After the dramatic decrease concurrent with TC passage, the SLA experiences a 20-day rapid exponential increase, followed by a slow increase. The response of mesoscale eddies to TCs reveals that COEs are enhanced by TCs in terms of a 24% (8%) increase in amplitude (circulation speed), and are enlarged in terms of a 19% increase in radius. Stronger or slower-moving TCs enhance COEs more significantly. In contrast, AOEs are weakened by TCs, with a 17% (8%) reduction in amplitude (circulation speed). The radius of AOEs is reduced by 13% on average. Nevertheless, the dependence of the AOE response on TC attributes is relatively weak. Overall, the response of COEs to TCs is generally more evident than that of AOEs, as evidenced by greater changes in the magnitude of eddy parameters.

The spatial pattern of TC-induced SST cooling reveals that COEs enhance the cooling, and this enhancement when COEs are located to the left of the TC track is more pronounced than that when COEs are located to the right. Compared with the cooling when there is no pre-existing eddy (referred to as COM condition), maximum cooling magnitude is increased by 61% and 26% when left COEs and right COEs pre-exist, respectively. The difference is primarily attributed to the combined effect of slow TC Uh and relatively sharp climatological background thermal stratification under left-COE condition. The pre-existing eddies also influence the location of the largest cooling, which shifts 40, 10, and 70 km rightwards off the TC track under COM, left-COE, and right-COE conditions, respectively. By contrast, AOEs suppress the SST cooling, and this suppression by right AOEs is a little stronger than that by left AOEs. Under left-AOE and right-AOE conditions, the largest cooling is suppressed by 33% and 42% in magnitude, which appears at 100 and 30 km to the right of the TC track, respectively. Furthermore, the enhancing (suppressing) effect of COEs (AOEs) on the cooling is more pronounced under stronger or slower-moving TCs. The eddy-modulated SST cooling is found to further feedback onto TC intensification. Compared with COM condition, COEs reduce TC intensification rate by 0.54 m s^{-1} per 24 hr (47%) on average, while AOEs increase it by 0.14 m s^{-1} per 24 hr (12%). Overall, the modulating effects of COEs on SST cooling and TC intensification are more evident than those of AOEs, and the modulating effects of left COEs are

stronger than right ones. The influence of the eddy location and eddy strength on TC intensity and rainfall pattern is more complex and will be detailed in our future studies (D. Y.-C.F Chen et al., 2011).

In short, our study systematically details the response of mesoscale eddies to TCs and the modulation of the TC-induced SST cooling and TC intensification by eddies over the SCS using satellite data. Nevertheless, the influence of eddies on the spatial pattern of cooling in global oceans remains unknown and needs to be studied in the future, considering different ocean environment conditions between the SCS and the open ocean (Mei et al., 2015). In addition, this study only focuses on the surface evolution of eddies affected by TCs, yet the vertical evolution of eddies remains unknown. Therefore, further studies utilizing mooring observations or numerical experiments are required to investigate the evolution of mesoscale eddies influenced by TCs and the potential influence of TCs on the ocean environment.

Data Availability Statement

The JTWC TC best-track data are obtained from the IBTrACS database (Knapp et al., 2018). The Mesoscale Eddy Trajectories Atlas product is produced by SSALTO/DUACS and distributed by AVISO+ (AVISO, 2023), with support from CNES, in collaboration with Oregon State University with support from NASA. The SLA data are available at the Copernicus Marine Service (CMEMS, 2023). The SST data are downloaded at the Remote Sensing Systems (RSS, 2023). The reanalysis wind data are obtained from the ECMWF ERA5 (Hersbach et al., 2023). Figures in this manuscript were made with Matlab software version R2022b (MATLAB, 2023).

Acknowledgments
This study is supported by the National Key Research and Development Program (project no. 2022YFC3104304), the National Natural Science Foundation of China (project nos. 42476029, 41876011, 42175007), the open research cruise NORC2023-05 supported by NSFC Shiptime Sharing Project (project no. 42249905), the Hainan Province Science and Technology Special Fund (project no. ZDYF2021SHFZ265), the State Key Laboratory of Tropical Oceanography, South China Sea Institute of Oceanology, Chinese Academy of Sciences (project no. LTO2321), and the Fundamental Research Funds for the Central Universities (project nos. 202001013129, 1901013184).

References

AVISO. (2023). Mesoscale Eddy Trajectory Atlas products merged version 2.0 delayed-time [Dataset]. *Archiving, Validation, and Interpretation of Satellite Oceanographic Data (AVISO)*. Retrieved from https://www.aviso.altimetry.fr/en/data/products/value-added-products/global-mesoscale-eddy-trajectory-product/meta2-0-dt.html

Balaguru, K., Foltz, G. R., Leung, L. R., D'Asaro, E., Emanuel, K. A., Liu, H., & Zedler, S. E. (2015). Dynamic Potential Intensity: An improved representation of the ocean's impact on tropical cyclones. *Geophysical Research Letters*, *42*(16), 6739–6746. https://doi.org/10.1002/2015gl064822

Balaguru, K., Leung, L. R., Lu, J., & Foltz, G. R. (2016). A meridional dipole in premonsoon Bay of Bengal tropical cyclone activity induced by ENSO. *Journal of Geophysical Research: Atmospheres*, *121*(12), 6954–6968. https://doi.org/10.1002/2016JD024936

Black, P. G., D'Asaro, E. A., Drennan, W. M., French, J. R., Niiler, P. P., Sanford, T. B., et al. (2007). Air–sea exchange in hurricanes: Synthesis of observations from the coupled boundary layer air–sea transfer experiment. *Bulletin of the American Meteorological Society*, *88*(3), 357–374. https://doi.org/10.1175/BAMS-88-3-357

Brand, S., & Blelloch, J. W. (1974). Changes in the characteristics of typhoons crossing the island of Taiwan. *Monthly Weather Review*, *102*(10), 708–713. https://doi.org/10.1175/1520-0493(1974)102<0708:CITCOT>2.0.CO;2

Carrère, L., Mertz, F., Dorandeu, J., Quilfen, Y., & Patoux, J. (2009). Observing and studying extreme low pressure events with altimetry. *Sensors*, *9*(3), 1306–1329. https://doi.org/10.3390/s90301306

Chelton, D. B., Schlax, M. G., & Samelson, R. M. (2011). Global observations of nonlinear mesoscale eddies. *Progress in Oceanography*, *91*(2), 167–216. https://doi.org/10.1016/j.pocean.2011.01.002

Chen, D. Y.-C., Cheung, K. K. W., & Lee, C.-S. (2011a). Some implications of core regime wind structures in western North Pacific tropical cyclones. *Weather and Forecasting*, *26*(1), 61–75. https://doi.org/10.1175/2010WAF2222420.1

Chen, G., Hou, Y., & Chu, X. (2011b). Mesoscale eddies in the South China Sea: Mean properties, spatiotemporal variability, and impact on thermohaline structure. *Journal of Geophysical Research*, *116*(C6), C06018. https://doi.org/10.1029/2010JC006716

Chiang, T.-L., Wu, C.-R., & Oey, L.-Y. (2011). Typhoon Kai-Tak: An ocean's perfect storm. *Journal of Physical Oceanography*, *41*(1), 221–233. https://doi.org/10.1175/2010JPO4518.1

CMEMS. (2023). SEALEVEL_GLO_PHY_L4_MY_008_047 [Dataset]. *Copernicus Marine Environment Monitoring Service (CMEMS), E.U. Copernicus Marine Service Information*. https://doi.org/10.48670/moi-00148

Cui, H., Tang, D., Liu, H., Sui, Y., & Gu, X. (2023). Composite analysis-based machine learning for prediction of tropical cyclone-induced Sea Surface height anomaly. *Ieee Journal of Selected Topics in Applied Earth Observations and Remote Sensing*, *16*, 1–10. https://doi.org/10.1109/JSTARS.2023.3247881

Cushman-Roisin, B., Tang, B., & Chassignet, E. P. (1990). Westward motion of mesoscale eddies. *Journal of Physical Oceanography*, *20*(5), 758–768. https://doi.org/10.1175/1520-0485(1990)020<0758:WMOME>2.0.CO;2

Dong, C., McWilliams, J. C., Liu, Y., & Chen, D. (2014). Global heat and salt transports by eddy movement. *Nature Communications*, *5*(1), 3294. https://doi.org/10.1038/ncomms4294

Emanuel, K. A. (1999). Thermodynamic control of hurricane intensity. *Nature*, *401*(6754), 665–669. https://doi.org/10.1038/44326

Emanuel, K. A. (2001). Contribution of tropical cyclones to meridional heat transport by the oceans. *Journal of Geophysical Research*, *106*(D14), 14771–14781. https://doi.org/10.1029/2000JD900641

Emanuel, K. A. (2003). Tropical cyclones. *Annual Review of Earth and Planetary Sciences*, *31*(1), 75–104. https://doi.org/10.1146/annurev.earth.31.100901.141259

Ferrari, R., & Wunsch, C. (2009). Ocean circulation kinetic energy: Reservoirs, sources, and sinks. *Annual Review of Fluid Mechanics*, *41*(1), 253–282. https://doi.org/10.1146/annurev.fluid.40.111406.102139

Foltz, G. R., Carton, J. A., & Chassignet, E. P. (2004). Tropical instability vortices in the Atlantic Ocean. *Journal of Geophysical Research*, *109*(C3), C03029. https://doi.org/10.1029/2003JC001942

Gray, W. M. (1968). Global view of the origin of tropical disturbances and storms. *Monthly Weather Review*, *96*(10), 669–700. https://doi.org/10.1175/1520-0493(1968)096<0669:GVOTOO>2.0.CO;2

Guan, S., Jin, F. F., Tian, J., Lin, I. I., Pun, I. F., Zhao, W., et al. (2024). Ocean internal tides suppress tropical cyclones in the South China Sea. *Nature Communications*, *15*(1), 3903. https://doi.org/10.1038/s41467-024-48003-y

Guan, S., Li, S., Hou, Y., Hu, P., Liu, Z., & Feng, J. (2018). Increasing threat of landfalling typhoons in the western North Pacific between 1974 and 2013. *International Journal of Applied Earth Observation and Geoinformation*, *68*, 279–286. https://doi.org/10.1016/j.jag.2017.12.017

Guan, S., Zhao, W., Huthnance, J., Tian, J., & Wang, J. (2014). Observed upper ocean response to typhoon Megi (2010) in the northern South China Sea. *Journal of Geophysical Research: Oceans*, *119*(5), 3134–3157. https://doi.org/10.1002/2013JC009661

Guan, S., Zhao, W., Sun, L., Zhou, C., Liu, Z., Hong, X., et al. (2021). Tropical cyclone-induced sea surface cooling over the Yellow Sea and Bohai Sea in the 2019 Pacific typhoon season. *Journal of Marine Systems*, *217*, 103509. https://doi.org/10.1016/j.jmarsys.2021.103509

Hersbach, H., Bell, B., Berrisford, P., Biavati, G., Horányi, A., Muñoz Sabater, J., et al. (2023). ERA5 hourly data on single levels from 1940 to present [Dataset]. *Copernicus Climate Change Service (C3S) Climate Data Store (CDS)*. https://doi.org/10.24381/cds.adbb2d47

Huang, X., & Wang, G. (2022). Response of a mesoscale dipole eddy to the passage of a tropical cyclone: A case study using satellite observations and numerical modeling. *Remote Sensing*, *14*(12), 2865. https://doi.org/10.3390/rs14122865

Jaimes, B., & Shay, L. K. (2009). Mixed layer cooling in mesoscale oceanic eddies during Hurricanes Katrina and Rita. *Monthly Weather Review*, *137*(12), 4188–4207. https://doi.org/10.1175/2009MWR2849.1

Jaimes, B., & Shay, L. K. (2010). Near-inertial wave wake of Hurricanes Katrina and Rita over mesoscale oceanic eddies. *Journal of Physical Oceanography*, *40*(6), 1320–1337. https://doi.org/10.1175/2010JPO4309.1

Jaimes, B., & Shay, L. K. (2015). Enhanced wind-driven downwelling flow in warm oceanic eddy features during the intensification of tropical cyclone Isaac (2012): Observations and theory. *Journal of Physical Oceanography*, *45*(6), 1667–1689. https://doi.org/10.1175/JPO-D-14-0176.1

Jansen, M. F., Ferrari, R., & Mooring, T. A. (2010). Seasonal versus permanent thermocline warming by tropical cyclones. *Geophysical Research Letters*, *37*(3). https://doi.org/10.1029/2009GL041808

Jin, W., Liang, C., Tian, X., Hu, J., Ding, T., Zhou, B., et al. (2022). Identifying oceanic responses with validated satellite observations after the passage of typhoons in the northern South China sea. *Remote Sensing*, *14*(16), 3872. https://doi.org/10.3390/rs14163872

Kimball, S. K., & Mulekar, M. S. (2004). A 15-year climatology of North Atlantic tropical cyclones. Part I: Size parameters. *Journal of Climate*, *17*(18), 3555–3575. https://doi.org/10.1175/1520-0442(2004)017<3555:AYCONA>2.0.CO;2

Knapp, K. R., Diamond, H. J., Kossin, J. P., Kruk, M. C., & Schreck, C. J. (2018). International best track archive for climate stewardship (IBTrACS) project (version 4) [Dataset]. *NOAA National Centers for Environmental Information*. https://doi.org/10.25921/82ty-9e16

Li, J., Yang, Y., Wang, G., Cheng, H., & Sun, L. (2021). Enhanced oceanic environmental responses and feedbacks to super Typhoon Nida (2009) during the sudden-turning stage. *Remote Sensing*, *13*(14), 2648. https://doi.org/10.3390/rs13142648

Li, Q., Sun, L., & Xu, C. (2018). The lateral eddy viscosity derived from the decay of oceanic mesoscale eddies. *Open Journal of Marine Science*, *8*(01), 152–172. https://doi.org/10.4236/ojms.2018.81008

Lin, I. I. (2012). Typhoon-induced phytoplankton blooms and primary productivity increase in the western North Pacific subtropical ocean. *Journal of Geophysical Research*, *117*(C3), C03039. https://doi.org/10.1029/2011JC007626

Lin, I.-I., Black, P., Price, J. F., Yang, C.-Y., Chen, S. S., Lien, C.-C., et al. (2013). An ocean coupling potential intensity index for tropical cyclones. *Monthly Weather Review*, *40*(9), 1878–1882. https://doi.org/10.1002/grl.50091

Lin, I. I., Liu, W. T., Wu, C.-C., Wong, G. T. F., Hu, C., Chen, Z., et al. (2003). New evidence for enhanced ocean primary production triggered by tropical cyclone. *Geophysical Research Letters*, *30*(13), 1718. https://doi.org/10.1029/2003gl017141

Lin, I. I., Wu, C.-C., Emanuel, K. A., Lee, I.-H., Wu, C.-R., & Pun, I.-F. (2005). The interaction of Supertyphoon Maemi (2003) with a warm ocean eddy. *Monthly Weather Review*, *133*(9), 2635–2649. https://doi.org/10.1175/MWR3005.1

Liu, F., & Tang, S. (2018). Influence of the interaction between typhoons and oceanic mesoscale eddies on phytoplankton blooms. *Journal of Geophysical Research: Oceans*, *123*(4), 2785–2794. https://doi.org/10.1029/2017JC013225

Liu, S., Sun, L., Wu, Q., & Yang, Y. (2017). The responses of cyclonic and anticyclonic eddies to typhoon forcing: The vertical temperature-salinity structure changes associated with the horizontal convergence/divergence. *Journal of Geophysical Research: Oceans*, *122*(6), 4974–4989. https://doi.org/10.1002/2017JC012814

Liu, Y., Guan, S., Lin, I. I., Mei, W., Jin, F. F., Huang, M., et al. (2023). Effect of storm size on sea surface cooling and tropical cyclone intensification in the western north Pacific. *Journal of Climate*, *36*(20), 7277–7296. https://doi.org/10.1175/JCLI-D-22-0949.1

Lloyd, I. D., & Vecchi, G. A. (2011). Observational evidence for oceanic controls on hurricane intensity. *Journal of Climate*, *24*(4), 1138–1153. https://doi.org/10.1175/2010JCLI3763.1

Lu, Z., & Shang, X. (2024). Limited width of tropical cyclone–induced baroclinic geostrophic response. *Journal of Physical Oceanography*, *54*(4), 1071–1088. https://doi.org/10.1175/JPO-D-23-0096.1

Lu, Z., Wang, G., & Shang, X. (2016). Response of a preexisting cyclonic ocean eddy to a typhoon. *Journal of Physical Oceanography*, *46*(8), 2403–2410. https://doi.org/10.1175/jpo-d-16-0040.1

Lu, Z., Wang, G., & Shang, X. (2020). Strength and spatial structure of the perturbation induced by a tropical cyclone to the underlying eddies. *Journal of Geophysical Research: Oceans*, *125*(5), e2020JC016097. https://doi.org/10.1029/2020jc016097

Lu, Z., Wang, G., Shang, X., & Xie, X. (2023). Uncertainties in altimetry observations of eddy changes induced by tropical cyclones. *Journal of Physical Oceanography*, *53*(1), 113–129. https://doi.org/10.1175/jpo-d-22-0115.1

Ma, Z. (2020). A study of the interaction between Typhoon Francisco (2013) and a cold-core eddy. Part I: Rapid weakening. *Journal of the Atmospheric Sciences*, *77*(1), 355–377. https://doi.org/10.1175/JAS-D-18-0378.1

Ma, Z., Fei, J., Huang, X., & Cheng, X. (2018). Modulating effects of mesoscale oceanic eddies on Sea Surface temperature response to tropical cyclones over the western North Pacific. *Journal of Geophysical Research: Atmospheres*, *123*(1), 367–379. https://doi.org/10.1002/2017jd027806

Ma, Z., Fei, J., Liu, L., Huang, X., & Li, Y. (2017). An investigation of the influences of mesoscale ocean eddies on tropical cyclone intensities. *Monthly Weather Review*, *145*(4), 1181–1201. https://doi.org/10.1175/MWR-D-16-0253.1

Ma, Z., Zhang, Z., Fei, J., & Wang, H. (2021). Imprints of tropical cyclones on structural characteristics of mesoscale oceanic eddies over the western North Pacific. *Geophysical Research Letters*, *48*(10), e2021GL092601. https://doi.org/10.1029/2021gl092601

MATLAB. (2023). MATLAB version R2022b [Software]. The MathWorks Inc. Retrieved from https://ww2.mathworks.cn/en/

Mei, W., Lien, C.-C., Lin, I. I., & Xie, S.-P. (2015). Tropical cyclone–induced ocean response: A comparative study of the South China Sea and tropical northwest Pacific. *Journal of Climate*, *28*(15), 5952–5968. https://doi.org/10.1175/JCLI-D-14-00651.1

Mei, W., & Pasquero, C. (2013). Spatial and temporal characterization of Sea Surface temperature response to tropical cyclones. *Journal of Climate*, *26*(11), 3745–3765. https://doi.org/10.1175/JCLI-D-12-00125.1

Mei, W., Primeau, F., McWilliams, J. C., & Pasquero, C. (2013). Sea surface height evidence for long-term warming effects of tropical cyclones on the ocean. *Proceedings of the National Academy of Sciences*, *110*(38), 15207–15210. https://doi.org/10.1073/pnas.1306753110

Nan, F., Xue, H., & Yu, F. (2015). Kuroshio intrusion into the South China sea: A review. *Progress in Oceanography*, *137*, 314–333. https://doi.org/10.1016/j.pocean.2014.05.012

Niwa, Y., & Hibiya, T. (1997). Nonlinear processes of energy transfer from traveling hurricanes to the deep ocean internal wave field. *Journal of Geophysical Research*, *102*(C6), 12469–12477. https://doi.org/10.1029/97jc00588

Powell, M. D., Vickery, P. J., & Reinhold, T. A. (2003). Reduced drag coefficient for high wind speeds in tropical cyclones. *Nature*, *422*(6929), 279–283. https://doi.org/10.1038/nature01481

Price, J. F. (1981). Upper ocean response to a hurricane. *Journal of Physical Oceanography*, *11*(2), 153–175. https://doi.org/10.1175/1520-0485(1981)011<0153:UORTAH>2.0.CO;2

Price, J. F. (1983). Internal wave wake of a moving storm. Part I. Scales, energy budget and observations. *Journal of Physical Oceanography*, *13*(6), 949–965. https://doi.org/10.1175/1520-0485(1983)013<0949:IWWOAM>2.0.CO;2

Price, J. F., Sanford, T. B., & Forristall, G. Z. (1994). Forced stage response to a moving hurricane. *Journal of Physical Oceanography*, *24*(2), 233–260. https://doi.org/10.1175/1520-0485(1994)024%3C0233:FSRTAM%3E2.0.CO;2

Pun, I.-F., Lin, I.-I., Lien, C.-C., & Wu, C.-C. (2018). Influence of the size of Supertyphoon Megi (2010) on SST cooling. *Monthly Weather Review*, *146*(3), 661–677. https://doi.org/10.1175/mwr-d-17-0044.1

Pun, I.-F., Lin, I. I., & Lo, M.-H. (2013). Recent increase in high tropical cyclone heat potential area in the Western North Pacific Ocean. *Geophysical Research Letters*, *40*(17), 4680–4684. https://doi.org/10.1002/grl.50548

Roemmich, D., & Gilson, J. (2001). Eddy transport of heat and thermocline waters in the North Pacific: A key to interannual/decadal climate variability? *Journal of Physical Oceanography*, *31*(3), 675–687. https://doi.org/10.1175/1520-0485(2001)031<0675:ETOHAT>2.0.CO;2

RSS. (2023). MW-IR optimum interpolated SST data set ver. 5.1 [Dataset]. *Remote Sensing Systems (RSS), PO.DAAC, CA, USA*. Retrieved from https://data.remss.com/SST/daily/mw_ir/v05.1/

Schlax, M. G., & Chelton, D. B. (2016). The "growing method" of eddy identification and tracking in two and three dimensions. *College of Earth, Ocean and Atmospheric, Oregon State University Sciences, Corvallis, Oregon*. Retrieved from https://www.aviso.altimetry.fr/fileadmin/documents/data/products/value-added/Schlax_Chelton_2016.pdf

Shang, X., Zhu, H., Chen, G., Xu, C., & Yang, Q. (2015). Research on cold core eddy change and phytoplankton bloom induced by typhoons: Case studies in the South China sea. *Advances in Meteorology*, *2015*, 1–19. https://doi.org/10.1155/2015/340432

Shay, L. K., & Chang, S. W. (1997). Free surface effects on the near-inertial ocean current response to a hurricane: A revisit. *Journal of Physical Oceanography*, *27*(1), 23–39. https://doi.org/10.1175/1520-0485(1997)027<0023:FSEOTN>2.0.CO;2

Shay, L. K., Goni, G. J., & Black, P. G. (2000). Effects of a warm oceanic feature on Hurricane Opal. *Monthly Weather Review*, *128*(5), 1366–1383. https://doi.org/10.1175/1520-0493(2000)128<1366:EOAWOF>2.0.CO;2

Sun, J., Ju, X., Zheng, Q., Wang, G., Li, L., & Xiong, X. (2023). Numerical study of the response of Typhoon Hato (2017) to grouped mesoscale eddies in the northern South China sea. *Journal of Geophysical Research: Atmospheres*, *128*(3), e2022JD037266. https://doi.org/10.1029/2022JD037266

Sun, L., Li, Y.-X., Yang, Y.-J., Wu, Q., Chen, X.-T., Li, Q.-Y., et al. (2014). Effects of super typhoons on cyclonic ocean eddies in the western North Pacific: A satellite data-based evaluation between 2000 and 2008. *Journal of Geophysical Research: Oceans*, *119*(9), 5585–5598. https://doi.org/10.1002/2013jc009575

Sun, L., Yang, Y.-J., & Fu, Y.-F. (2009). Impacts of typhoons on the Kuroshio large meander: Observation evidences. *Atmospheric and Oceanic Science Letters*, *2*(1), 45–50. https://doi.org/10.1080/16742834.2009.11446772

Sun, L., Yang, Y.-J., Xian, T., Lu, Z., & Fu, Y. (2010). Strong enhancement of chlorophyll a concentration by a weak typhoon. *Marine Ecology Progress Series*, *404*, 39–50. https://doi.org/10.3354/meps08477

Vincent, E. M., Lengaigne, M., Madec, G., Vialard, J., Samson, G., Jourdain, N. C., et al. (2012). Processes setting the characteristics of sea surface cooling induced by tropical cyclones. *Journal of Geophysical Research*, *117*(C2), C02020. https://doi.org/10.1029/2011jc007396

Walker, N. D., Leben, R. R., & Balasubramanian, S. (2005). Hurricane-forced upwelling and chlorophyll a enhancement within cold-core cyclones in the Gulf of Mexico. *Geophysical Research Letters*, *32*(18), L18610. https://doi.org/10.1029/2005gl023716

Walker, N. D., Leben, R. R., Pilley, C. T., Shannon, M., Herndon, D. C., Pun, I.-F., et al. (2014). Slow translation speed causes rapid collapse of northeast Pacific Hurricane Kenneth over cold core eddy. *Geophysical Research Letters*, *41*(21), 7595–7601. https://doi.org/10.1002/2014gl061584

Wang, G., Ling, Z., & Wang, C. (2009). Influence of tropical cyclones on seasonal ocean circulation in the South China Sea. *Journal of Geophysical Research*, *114*(C10), C10022. https://doi.org/10.1029/2009jc005302

Wang, G., Su, J., & Chu, P. C., (2003). Mesoscale eddies in the South China Sea observed with altimeter data. *Geophysical Research Letters*, *30*(21), 2121. https://doi.org/10.1029/2003GL018532

Wang, G., Su, J., Ding, Y., & Chen, D. (2007). Tropical cyclone genesis over the South China sea. *Journal of Marine Systems*, *68*(3–4), 318–326. https://doi.org/10.1016/j.jmarsys.2006.12.002

Wang, G., Wu, L., Johnson, N., & Ling, Z. (2016). Observed three-dimensional structure of ocean cooling induced by Pacific tropical cyclones. *Geophysical Research Letters*, *43*(14), 7632–7638. https://doi.org/10.1002/2016gl069605

Wang, Y. (2020). Composite of typhoon-induced Sea Surface temperature and chlorophyll-a responses in the South China sea. *Journal of Geophysical Research: Oceans*, *125*(10), e2020JC016243. https://doi.org/10.1029/2020JC016243

Wang, Y., & Xiu, P. (2022). Typhoon footprints on ocean surface temperature and chlorophyll-a in the South China Sea. *Science of the Total Environment*, *840*, 156686. https://doi.org/10.1016/j.scitotenv.2022.156686

Wu, C.-C., Lee, C.-Y., & Lin, I. I. (2007). The effect of the ocean eddy on tropical cyclone intensity. *Journal of the Atmospheric Sciences*, *64*(10), 3562–3578. https://doi.org/10.1175/JAS4051.1

Ye, H., Ma, Z., Fei, J., & Duan, Y. (2023). Evaluation of leftward biased cold wakes induced by tropical cyclones in the North Hemisphere. *Journal of Geophysical Research: Oceans*, *128*(12), e2023JC020188. https://doi.org/10.1029/2023JC020188

Zhan, W., He, Q., Zhang, Y., & Zhan, H. (2022). Anticyclone eddies favor the genesis of off-season tropical cyclone in the western North Pacific. *Journal of Geophysical Research: Atmospheres*, *128*(1), e2022JD036945. https://doi.org/10.1029/2022JD036945

Zhang, H., Liu, Y., Liu, P., Guan, S., Wang, Q., Zhao, W., & Tian, J. (2023a). Enhanced upper ocean response within a warm eddy to Typhoon Nakri (2019) during the sudden-turning stage. *Deep Sea Research Part I: Oceanographic Research Papers*, *199*, 104112. https://doi.org/10.1016/j.dsr.2023.104112

Zhang, Y., Liu, Y., Guan, S., Wang, Q., Zhao, W., & Tian, J. (2023b). Sudden track turning of Typhoon Prapiroon (2012) enhanced the upper ocean response. *Remote Sensing*, *15*(2), 302. https://doi.org/10.3390/rs15020302

Zhang, Y., Zhang, Z., Chen, D., Qiu, B., & Wang, W. (2020). Strengthening of the Kuroshio current by intensifying tropical cyclones. *Science*, *368*(6494), 988–993. https://doi.org/10.1126/science.aax5758

Zhang, Z., Tian, J., Qiu, B., Zhao, W., Chang, P., Wu, D., & Wan, X. (2016). Observed 3D structure, generation, and dissipation of oceanic mesoscale eddies in the South China sea. *Scientific Reports*, *6*(1), 24349. https://doi.org/10.1038/srep24349

Zhang, Z., Wang, W., & Qiu, B. (2014). Oceanic mass transport by mesoscale eddies. *Science*, *345*(6194), 322–324. https://doi.org/10.1126/science.1252418

Zheng, Z.-W., Ho, C.-R., & Kuo, N.-J. (2008). Importance of pre-existing oceanic conditions to upper ocean response induced by Super Typhoon Hai-Tang. *Geophysical Research Letters*, *35*(20), L20603. https://doi.org/10.1029/2008GL035524

Zheng, Z.-W., Ho, C.-R., Zheng, Q., Lo, Y.-T., Kuo, N.-J., & Gopalakrishnan, G. (2010). Effects of preexisting cyclonic eddies on upper ocean responses to Category 5 typhoons in the western North Pacific. *Journal of Geophysical Research*, *115*(C9), C09013. https://doi.org/10.1029/2009jc005562